European Journal of Medicinal Chemistry 295 (2025) 117799

Contents lists available at ScienceDirect

European Journal of Medicinal Chemistry

journal homepage: www.elsevier.com/locate/ejmech

Research paper

Exploiting acylaminopyrazole scaffold for polypharmacology approach in Alzheimer's disease

Rebecca Orioli [a,1], Giuliana Sarno [b,1], Francesca Seghetti [a,2], Silvia Gobbi [a], Federica Belluti [a], Alessandra Feoli [b], Francesca Massenzio [c], Barbara Monti [c,d], Rosaria Spagnuolo [a], Manuela Bartolini [a], Sabrina Castellano [b,**], Alessandra Bisi [a,*]

[a] Department of Pharmacy and Biotechnology, Alma Mater Studiorum-University of Bologna, Via Belmeloro 6, 40126 Bologna, Italy
[b] Department of Pharmacy, Università degli Studi di Salerno, Via Giovanni Paolo II, 132, 84084 Fisciano SA, Italy
[c] Department of Pharmacy and Biotechnology, Alma Mater Studiorum-University of Bologna, Via Selmi 3, 40126, Bologna, Italy
[d] IRCCS Istituto delle Scienze Neurologiche di Bologna, Bologna, Italy

ARTICLE INFO

Keywords:
Aminopyrazole
GSK-3β
Chelating agents
Neuroprotection

ABSTRACT

Neurodegenerative diseases currently represent one of the most serious health pitfalls for the world population. Considering their multifactorial nature, research has focused on the study of small molecules able to simultaneously tackle different targets involved in their onset and progression. In this paper, two sets of acylaminopyrazole-based compounds were designed to exploit the aminopyrazole core as a privileged structure properly decorated with an acyl moiety and a further amide function, connected with a proper spacer. Indeed, acylated aminopyrazoles could be able to establish the appropriate hydrogen bond pattern to both bind GSK-3β, responsible for tau hyperphosphorylation, prevent the formation of insoluble Aβ-protein aggregates and have the structural features to show chelating properties towards metals involved in neuroinflammation. The collection of compounds was tested *in vitro* for GSK-3β inhibition activity, antiaggregating and chelating properties. Selected compounds were able to inhibit GSK-3β in the low micromolar range with a reversible and competitive mechanism of action, as established by Microfluidic Mobility Shift Assay (MMSA) and showed metal chelating ability. Preliminary Structure Activity Relationships (SARs) to hit these distinct and interconnected targets for neuromodulation were established. Finally, selected compounds showed good apparent permeability values in parallel artificial membrane permeability assay (PAMPA) together with good cellular safety profile. The collected results validated acylaminopyrazole as promising scaffold for the development of multitarget-directed ligands. Compounds **1c** and **4c** emerged as promising prototypes, and deserve further optimization in the search for drug candidates for polypharmacological approach in neurodegenerative disease.

1. Introduction

Due to the progressive increase in life expectancy, the need for drugs designed to treat chronic neurodegenerative diseases (NDs) is becoming increasingly urgent. Unfortunately, because of the heterogeneity of pathologies linked to the central nervous system (CNS), timely diagnosis and efficient medical intervention are challenging. Moreover, the multiple and networked targets involved in the onset and progression of NDs constitute a further critical issue in the development of disease-modifying drugs. A polypharmacology approach may then be seen as a valuable strategy for addressing these multifaceted diseases, by simultaneously affecting different pathways involved in their unpreventable advancement. The search for new validated targets to be engaged by small-molecule drugs represents one of the main challenges in combating NDs [1].

About 60–70 % of the cases of dementia in elderly people can be

* Corresponding author.
** Corresponding author.
E-mail addresses: scastellano@unisa.it (S. Castellano), alessandra.bisi@unibo.it (A. Bisi).
[1] Co-first authors.
[2] Present address: Autifony Srl, Istituto di ricerca pediatrica Città della Speranza, Via Corso Stati Uniti 4f, 35127 Padua, Italy-e-mail: francesca.seghetti@autifony.com

https://doi.org/10.1016/j.ejmech.2025.117799
Received 19 March 2025; Received in revised form 21 May 2025; Accepted 22 May 2025
Available online 25 May 2025

ascribed to Alzheimer's Disease (AD). This ND leads to a progressive impairment in brain cognitive functions, and the molecular mechanisms of its onset and progression are still largely unknown. Two evident and recognized hallmarks of this pathology are the accumulation of extracellular amyloid β (Aβ) plaques, formed by insoluble oligomers of the Aβ peptide, and of intracellular neurofibrillary tangles (NFTs), constituted by hyperphosphorylated tau protein. Tau is a microtubule-associated protein involved in the regulation of microtubules stability and axonal transport in the brain, and considering that microtubules maintain the cytoskeleton of neurons, a disruption of this system due to the hyperphosphorylation of tau protein inevitably leads to cell function impairment [2]. Beside Aβ and tau aggregation, neuroinflammation is another major feature of AD brain pathology often observed in the early stages of the disease, and even prior to the formation of amyloid plaques [3]. Due to this complex picture, there is currently no cure for AD, but symptomatic drugs, such as cholinesterase inhibitors and the NMDA receptor antagonist Memantine, are available and often used in combination. In 2023 and 2024, the Food and Drug Administration approved two monoclonal antibodies, Lecanemab and Donanemab, able to remove Aβ plaques and prevent the formation of aggregates. Their efficacy is not yet fully established, and further issues about safety and efficacy, especially considering their use for long periods, remain to be clarified [4]. Since one of the main risk factors for the development of AD is advanced age, and considering the progressive aging of the world population, the search for new targets to be engaged appears of fundamental importance.

Protein kinases (PKs), mediating protein phosphorylation, play a key role in regulating crucial cellular functions, namely cell proliferation, differentiation, metabolism and apoptosis, and their overexpression has been frequently reported in many pathological conditions, thus representing a possible mechanism of disease development. Hence, small-molecule kinase inhibitors hold promises in treating several disorders, including cancer, inflammation, cardiovascular diseases, and NDs. One of the most investigated PKs in AD physiopathology is glycogen synthase kinase 3β (GSK-3β), a serine/threonine kinase ubiquitously expressed and critically involved in multiple cellular functions. Remarkably, GSK-3β is also widely found in the CNS and its dysregulation has been related to tau phosphorylation, Aβ accumulation, reduced synaptic plasticity and inflammation [5]. The catalytic domain of GSK-3β is structurally organized in two lobes: the smaller N-terminal lobe is mainly formed by β-sheets and one preserved α-helix (C-helix), while the larger C-terminal lobe is mainly formed by alpha-helixes and comprises the activation segment, containing residues that are usually phosphorylated upon kinase activation. The two lobes are connected through the hinge region, and ATP binds in the folding cleft between the two lobes, by means of conserved hydrogen bond interactions with the hinge [6]. Since GSK-3β catalyses the transfer of a phosphate group from ATP to the substrate, the development of inhibitors targeting the ATP binding site represents a valuable inhibition strategy in drug discovery [7]. Hence, for the design of potent ATP competitive inhibitors, the formation of a network of hydrogen bond interactions with the kinase hinge region with properly selected scaffolds is a widely accepted approach, and many putative hinge-binding fragments have been identified by mapping the core structure of known inhibitors into kinase pharmacophore models. In this respect, privileged structures, i.e. chemical frameworks endowed with activities against different targets when properly decorated, have been widely exploited in developing enzyme inhibitors. Among those, the pyrazole scaffold has emerged as an important building block, being endowed with beneficial ancillary properties [8]. Indeed, acylated aminopyrazoles were shown to be able to prevent the formation of insoluble Aβ-protein aggregates, thanks to a donor-acceptor-donor (DAD) hydrogen bond pattern complementary to that of the β-sheet portions in Aβ (Fig. 1) [9,10]. Likewise, the acetamido-pyrazole fragment has been identified as a promising ligand for the hinge region of GSK-3β in a hit discovery campaign performed by virtual ligand screening [11]. Furthermore, the pyrazole scaffold is recognized to be able to form coordination bonds with varius metals [12] and it could be exploited as chelating agent and properly functionalized to target biometals in AD. These considerations suggest that an acylated aminopyrazole could be a suitable scaffold for a polypharmacological approach in AD treatment.

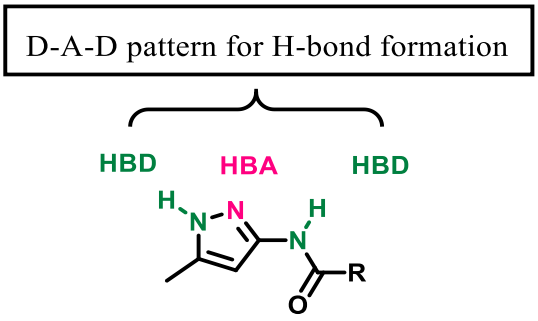

Fig. 1. H-bond network of acylaminopyrazole derivatives. HBD: H-bond donor; HBA: H-bond acceptor.

2. Design

In this paper we report the design and synthesis of a series of acylated aminopyrazole derivatives featuring an additional terminal amide group. The amide function is found in many biologically active molecules, including peptides and proteins, and plays a significant role in forming hydrogen bond interactions with the biological target. Moreover, due to its similarity with the peptide bond, the presence of an amide moiety could enhance the interaction with the oligomeric sequence of Aβ fragments, reducing their propensity to aggregate [13]. The acylated aminopyrazole scaffold was then connected, through a proper spacer, with a *N*-methylbenzyl terminal moiety, to evaluate the ability of a planar and relatively bulky aromatic group to enter the ATP-binding site of GSK-3β and concurrently interfere with Aβ aggregation (Fig. 2). To evaluate the impact of length, flexibility, and/or rigidity of the linker chain on GSK-3β inhibitory activity, the rigid maleic (*cis*, **1a-c**) and fumaric (*trans*, **2a-c**) acids and the flexible succinic (**3a-c**) and glutaric (**4a-c**) acids were selected. Moreover, the two amide functions were also directly connected through an oxalic acid fragment (**5a-c**). The *N*-methylbenzyl terminal moiety was initially left unmodified (**1a-5a**), or functionalized with *p*-OCH_3 (**1b**–**5b**) and *p*-Cl (**1c-5c**).

Based on the inhibitory potencies observed for these derivatives towards GSK-3β, indicating **1c** as the best compound of the series, a second set of analogues was designed (**1d-j**, Fig. 2), for a better assessment of the structure-activity relationships (SARs). The maleic linker was preserved, and decoration of the phenyl ring of the benzylamide moiety with substituents featuring different electronic and steric properties was performed. Moreover, the *N*-methyl substituent was removed (compound **1k**), to evaluate the effect elicited by an additional hydrogen-donor group.

The new derivatives were evaluated for GSK-3β inhibitory activity and their ability to counteract Aβ aggregation and neuroinflammation *in vitro*. Moreover, considering the peculiar core structure of the compounds, the potential chelating properties of the most active derivatives were also assessed. Indeed, the homeostasis of biometals such as copper, iron, zinc, and manganese is impaired in AD [14], and the resulting overload of these metals seems to promote oxidative stress and tau and Aβ aggregation.

3. Results

3.1. Chemistry

The synthetic strategy to obtain compounds **1a-c**, **2a-c**, **3a-c**, **4a-c**,

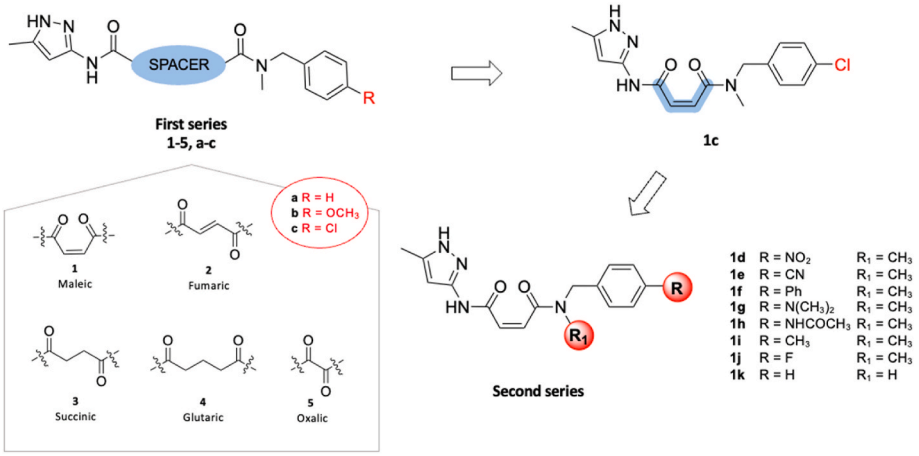

Fig. 2. Design strategy for the aminopyrazole derivatives.

and **5a-c** is depicted in Scheme 1. Starting from benzylamines reported in the literature or commercially available, several strategies were followed to introduce the desired linker. Compounds **7a-c**, **8a-c**, and **9a-c** were synthesized by treating the commercially available *N*-methyl-1-phenylmethanamine **6a**, the 1-(4-methoxyphenyl)-*N*-methylmethanamine **6b** [15] or the 1-(4-chlorophenyl)-*N*-methylmethanamine **6c** [15] with maleic, succinic or glutaric anhydride, in the presence of triethylamine. Compounds **10a-c** were prepared by coupling reaction between the *N*-benzylmethylamines **6a-c** and fumaric acid, in the presence of HATU and DIPEA. Compounds **11a-c** were obtained through a *N*-acylation reaction between ethyloxalylchloride and amines **6a-c**, followed by the saponification of the ethyl ester function by lithium hydroxide. Finally, compounds **1a-c**, **2a-c**, **3a-c**, **4a-c** and **5a-c** were obtained via a coupling reaction between carboxylic acids **7a-c**, **8a-c**, **9a-c**, **10a-c**, **11a-c** and 3-methyl-5-aminopyrazole.

A convergent synthetic approach was performed to increase efficiency, thus obtaining the second series of compounds (**1d-k**) (Scheme 2). The reaction of maleic anhydride with methylaminopyrazole straightforwardly yielded compound **12**, which was then coupled with the *p*-substituted benzylamines **6d-k** to achieve the target compounds. Except for the commercially available **6k**, the *N*-methylbenzylamines **6d-j** were prepared as reported in literature [15–20].

It is well known that secondary and tertiary amides, due to the partial double-bond character of the amide C–N bond, could lead to *cis* and *trans* rotamers that usually cannot be isolated due to the low-energy barrier of conversion between the two conformations. However, NMR spectroscopy studies can help to determine the structural ratios of *cis-trans* rotamers for most amide derivatives [21]. Accordingly, NMR spectra of the new compounds showed typical patterns of a mixture of *cis-trans* isomers, with proton and carbon signals of the *N*-methyl amide moiety and of the methylene near the carbonyl group appearing as overlapping double peaks, following for the proton signals the ratio 2:1, in agreement with literature [22].

3.2. Biological evaluation

3.2.1. Solubility determination

Assays artifacts, such as false positives due to aggregates, can be partially related to the low solubility of the compounds. Therefore, to establish the appropriate concentration range to be tested and to ascertain whether the compounds have solubility issues, their solubility profiles were determined in aqueous solutions with 2 % DMSO using nephelometric measurements. In detail, two concentrations (100 and 200 μM) were tested in PBS buffer within a time frame (0, 30, 60 and 90 min). All compounds displayed good solubility at both tested concentrations (SI, Fig. S1).

3.2.2. In vitro GSK-3β inhibitory activity

The evaluation of the inhibitory activities of compounds toward GSK-3β was performed employing the LANCE Ultra TR-FRET assay, one of the well-established methods to determine kinase activity [23]. First, all compounds were tested at two fixed doses (2 and 20 μM) to verify the

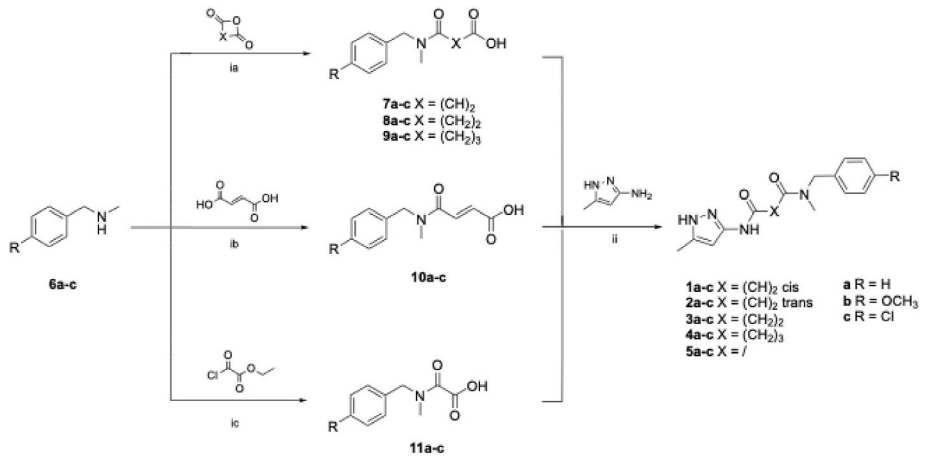

Scheme 1. Synthesis of compounds **1a-c**, **2a-c**, **3a-c**, **4a-c** and **5a-c**. ia) NEt_3, DCM, 7 h, r.t. 50–98 %; ib) HATU, DIPEA, DMF, 2 h, r.t. 56–100 %; ic) DIPEA, DCM, 3.5 h, 0 °C to r.t., then LiOH, THF/H_2O 1:1, 6 h, r.t. 88–97 %; ii) HATU, DIPEA, DMF, 4–18 h, r.t, 29–77 %.

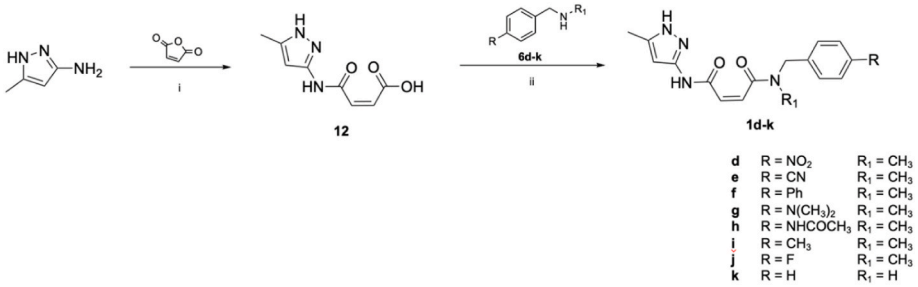

Scheme 2. Synthesis of compounds **1d-k**. i) NEt_3, DCM, r.t., 1 h, 89 %; ii) HATU, DIPEA, DMF, 2 h, r.t., 17–41 %.

dose-dependent inhibition effect. Then, for compounds with an inhibition activity of GSK-3β higher than 90 % at 20 μM and higher than 20 % at 2 μM, IC_{50} values were determined. Percent inhibition data and IC_{50} data are reported in Table 1 and in Table 2, whereas IC_{50} curves were detailed in supporting information Fig. S2.

The first series of compounds (**1a-c**, **2a-c**, **3a-c**, **4a-c**, and **5a-c**) was tested in order to establish the most appropriate linker for obtaining significant GSK-3β inhibition (Table 1). Maleic-based compounds **1d-k** were also evaluated to assess the role of the substituent on the *N*-benzyl group (Table 2).

Looking at the results of the first set of pyrazole-based derivatives (**1–5 a-c**, Table 1), the maleic linker, bearing a double bond in a *cis* configuration, appeared the most suitable one, leading to compounds **1a-c** that showed IC_{50} values in the low micromolar range (5.9, 2.4 and 2.2 μM, respectively). In this regard, this spacer emerged as more appropriate than the corresponding *trans* analogue fumaric (**2a-c**), leading to the speculation that a definite spatial orientation of the two amide groups can provide a suitable interaction with the binding cleft of GSK-3β. This consideration was corroborated by the appreciable results obtained with compounds bearing the more flexible succinic (**3c**, IC_{50} = 10.1 μM) and glutaric linkers (**4c**, IC_{50} = 3.4 μM), whose conformational flexibility likely allowed a proper spatial arrangement of the pharmacophoric moieties, allowing them to accommodate into the enzyme binding cleft, similarly to **1c**. Notably, in addition to the *trans* fumaric, the oxalic linker led to inactive derivatives as well, maybe due to the lack of the appropriate spatial distribution of the two moieties. As regards substituents on the *N*-methylbenzyl terminal moiety, besides the unsubstituted compound, *p*-OCH_3 and *p*-Cl were initially selected, on the basis of their differences in both lipophilic and electronic properties. The inhibitory activities of the most active maleic-based derivatives **1a-c** showed that a two-fold increase in activity was observed with the introduction in *para* position of both OCH_3 (**1b**) and Cl (**1c**), compared with the unsubstituted **1a**, despite their different physico-chemical properties. Nevertheless, a closer look at all the results highlighted a more favourable contribution for the Cl atom, in particular for derivatives bearing a spacer different from the maleic one, such as a linear alkyl tether (compounds **3c** and **4c**).

For a better assessment of this feature, in the second series of compounds **1d-k**, substituents endowed with unrelated lipophilic and electronic properties were introduced in the *para* position of the benzyl function, while keeping the preferred maleic spacer. As reported in Table 2, except for the *p*-CH_3 substituted **1i**, the best results were

Table 1
Inhibition of GSK-3β enzymatic activity of the first series of compounds (**1a-c**, **2a-c**, **3a-c**, **4a-c**, **5a-c**). For compounds having a significant percentage inhibition activity (i.a.), IC_{50} values were determined. n.i. no inhibition was observed at the tested concentrations. n.t. not tested.

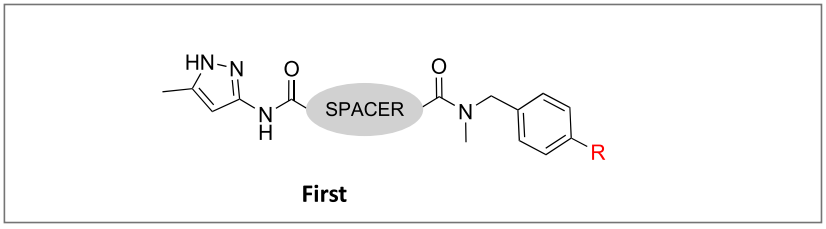

Compound	R	i.a. % 20 μM[a]	i.a. % 2 μM[a]	IC_{50} μM[b]
1a	H	97.5 ± 2.1	37.0 ± 0.1	5.9
1b	OCH_3	99.5 ± 1.9	74.2 ± 5.3	2.4
1c	Cl	100.6 ± 0.9	62.7 ± 8.2	2.2
2a	H	79.6 ± 3.9	7.4 ± 10.4	n.t.
2b	OCH_3	76.3 ± 2.2	n.i.	n.t.
2c	Cl	90.7 ± 2.1	n.i.	n.t.
3a	H	74.7 ± 14.5	7.9 ± 0.9	n.t.
3b	OCH_3	77.0 ± 7.0	14.3 ± 15.9	n.t.
3c	Cl	90.6 ± 0.5	40.4 ± 6.8	10.1
4a	H	85.3 ± 0.4	18.4 ± 11.4	n.t.
4b	OCH_3	79.7 ± 0.1	6.1 ± 2.3	n.t.
4c	Cl	98.3 ± 0.8	49.7 ± 4.4	3.4
5a	H	n.i.	n.i.	n.t.
5b	OCH_3	16.6 ± 8.5	n.i.	n.t.
5c	Cl	24.1 ± 6.2	5.7 ± 12.5	n.t.
SB216763				0.0114

[a] Values obtained for each compound are the means ± SD determined for two independent experiments.
[b] The compounds were tested in 10 doses with 2-fold serial dilutions in singlicate format. IC_{50} curves are depicted in Fig. S2.

Table 2
Inhibition of GSK-3β enzymatic activity of the second series of compounds (**1d-k**). For compounds having significant activity, IC_{50} values are also listed. n.i. no inhibition at tested concentrations. n.t. not tested.

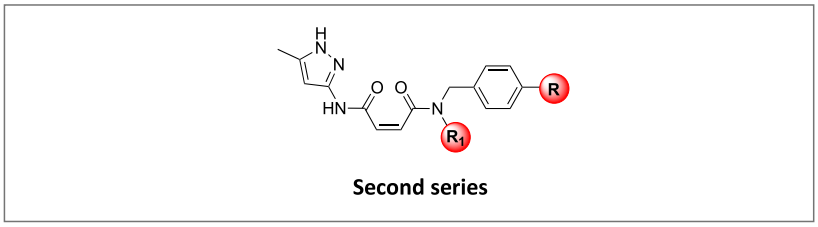

Second series

Compound	R	R_1	i.a. % 20 μM[a]	i.a. % 2 μM[a]	IC_{50} μM[b]
1d	NO_2	CH_3	89.3 ± 3.0	18.8 ± 2.2	5.9
1e	CN	CH_3	95.7 ± 0.6	33.6 ± 1.8	3.1
1f	Ph	CH_3	88.8 ± 2.9	22.3 ± 0.9	n.t.
1g	$N(CH_3)_2$	CH_3	35.3 ± 1.4	7.0 ± 1.7	n.t.
1h	$NHCOCH_3$	CH_3	73.7 ± 8.4	21.9 ± 17.5	n.t.
1i	CH_3	CH_3	91.5 ± 2.2	23.4 ± 4.5	4.4
1j	F	CH_3	97.2 ± 1.5	48.3 ± 3.4	3.3
1k	H	H	74.3 ± 1.4	15.5 ± 3.8	n.t.
SB216763					0.0114

[a] Values obtained for each compound are the means ± SD determined for two independent experiments.
[b] The compounds were tested in 10 doses with 2-fold serial dilutions in singlicate format. IC_{50} curves are depicted in Figure S2

obtained with electron-withdrawing substituents, namely NO_2, CN and F (**1d**, **1e** and **1j**, respectively), in line with the data observed for the most active compound, *i.e.* the *p*-Cl derivative **1c**. This result appeared even more significant when compared with the low inhibitory activity of compound **1g**, bearing a *p*-dimethylammino moiety, which proved to be the least potent derivative in the series. Notably, the introduction of a further amide function (*p*-acetamide), as in compound **1h**, had a negligible effect on the inhibitory potency. Finally, the presence of the *N*-methyl amide moiety seemed favourable for activity, being compound **1k** less potent than **1a**. Taken together, the results obtained from the inhibition experiments of the full collection of compounds allowed to establish preliminary SARs for this new chemotype, to enable the future design of related derivatives to obtain compounds able to hit each target to an appropriate extent.

3.2.3. *Mechanism of action studies*

Once the SARs for GSK-3β inhibition were defined, our attention turned to the characterization of the mode of interaction of this class of compounds with the enzyme. Mechanism of Action (MOA) studies are fundamental in a drug discovery process, as they can be used to establish if the inhibition is reversible or irreversible and if the discovered inhibitor has a competitive, noncompetitive or uncompetitive behavior and, therefore, foresee liabilities associated with the mechanism. To perform MOA analysis, we selected compound **1c** and exploited Microfluidic Mobility Shift Assay (MMSA). MMSA is a technique that combines the fundamental principles of electrophoresis and mobility shift via a microfluidic chip system. The microscopic quartz channels of the chip serve as the separation matrix, enabling the electrophoretic separation of fluorescently labeled molecules through a pressure-driven fluidic flow and a difference in electrical potential [24]. An essential advantage of this assay is that neither secondary reagents (e.g., antibodies) nor secondary enzymes are required for detection, and potential interference by fluorescent compounds can be detected and minimized by changing the separation conditions of electrophoresis. The literature reports the use of MMSA for studying different classes of enzymes [25–30]. The more comprehensive application is for those classes of enzymes, such as kinases, phosphatases, proteases, and phosphodiesterases, that lead to the formation of a product with a clear difference in charge/mass (z/m) ratio with respect to the substrate [31–33]. Moreover, the ability to monitor enzymatic reactions in real-time facilitates the kinetic study, making it an intriguing technique for assessing the mechanism of action of putative inhibitors [27,34,35].

Preliminary, we evaluated and characterized all the parameters (i.e., reaction buffer composition, enzyme, substrate, and co-factor concentrations) involved in the enzymatic reaction and in the electrophoretic separation to define the appropriate assay conditions (SI, Figs. S3–5). Subsequently, compound SB216763, a well-known ATP-competitive inhibitor [36–38] was used to validate the assay (SI, Figs. S6–9).

The IC_{50} value of compound **1c** was also evaluated by MMSA, since it is required for the MOA investigation experiments. The IC_{50} value obtained (1.56 ± 0.30 μM, Fig. S10) turned out to be comparable with the one provided by FRET assay (2.2 μM).

Remarkably, the electrophilic double bond in compound **1c** could be susceptible to covalent interactions, leading to an irreversible inhibition of the enzyme. To leave out this hypothesis, MMSA was exploited. First, GSK-3β, at 100-fold the concentration required for the assay, was incubated with **1c** at 10-fold IC_{50} concentration to achieve a percentage of inhibition greater than 80 %. After 60 min, the sample was diluted 100-folds into assay buffer, containing the enzyme substrate. The plots of activity as a function of time (progress curves) were then generated for untreated and **1c** treated samples. Data presented in Fig. 3 indicated that, after dilution, the enzymatic activity was restored, therefore supporting a reversible mechanism of inhibition by compound **1c**.

To substantiate this outcome, we also performed a Jump-Dilution experiment by TR-FRET [39]. As described for the MMSA assay, GSK-3β, at 100-fold the concentration required for the assay, was incubated with **1c** at 10-fold $IC_{50,}$ and after 30 min a 100-fold dilution into activity assay buffer was performed.

Results reported in Fig. 4 indicated the restoration of GSK-3β activity after dilution, confirming the reversibility of GSK-3β inhibition by **1c**.

Once assessed the reversible mode of action of **1c**, we moved to MOA studies to establish the type of inhibition for compound **1c** (competitive, noncompetitive, or uncompetitive). First, we used four different concentrations of ATP (36 μM, 18 μM, 9 μM, and 4.5 μM) while keeping the concentration of compound **1c** fixed at its IC_{50} value, and inhibition was evaluated after 60 min of incubation. Results depicted in Fig. 5 clearly showed a reduction of inhibitory activity with increasing ATP concentrations, highlighting an ATP-competitive mechanism of inhibition for compound **1c**.

To corroborate this assumption, we performed double titration

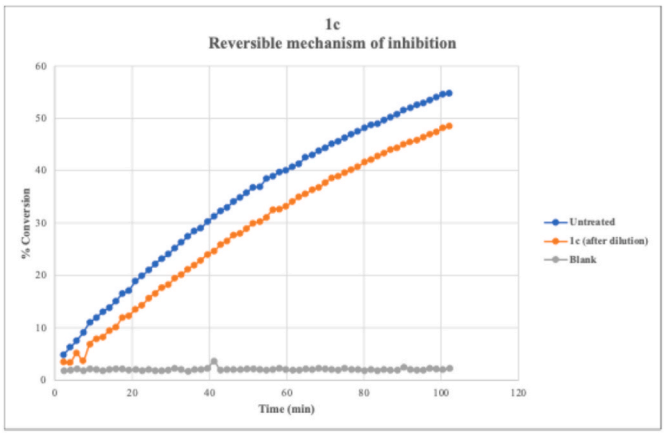

Fig. 3. Reversible mechanism of inhibition of compound **1c**. Progress curves for the sample treated with inhibitor **1c** after dilution at the IC_{50} concentration (orange dots), and for both untreated (blue dots) and blank (grey dots, buffer without co-factor) samples. (For interpretation of the references to colour in this figure legend, the reader is referred to the Web version of this article.)

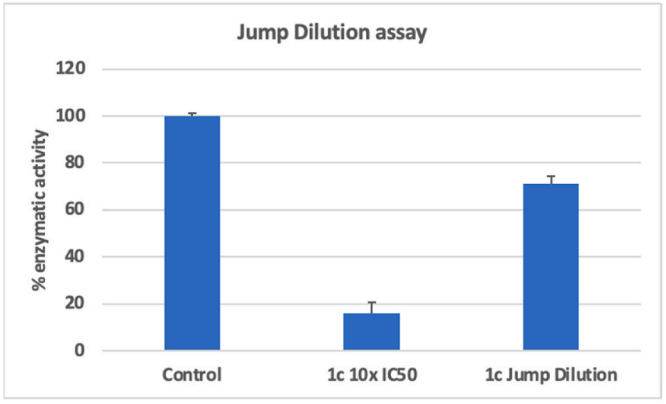

Fig. 4. Jump-Dilution experiment by TR-FRET. GSK-3β (100x concentration) was incubated with **1c** (10x IC_{50}) to achieve an inhibition greater than 80 %. The 100-fold dilution of the sample restored the enzymatic activity.

experiments, simultaneously changing **1c** and ATP concentrations. We selected six concentrations for **1c** (3.13, 1.56, 0.78, 0.39, 0.20, and 0.10 μM) and five for ATP (36, 18, 9, 4.50, and 2.25 μM) and the reaction was kinetically monitored (every 2 min for ~70 min). K_M and V_{max} parameters were calculated by fitting reaction rates at each ATP concentration to the Michaelis-Menten equation (Fig. 6A). Subsequently, K_M and V_{max} were plotted against increasing concentrations of inhibitor **1c** (Fig. 6B and C). These findings supported the assumption of a competitive behavior of **1c**, as K_M increased linearly with inhibitor concentrations while V_{max} remained unchanged. Double-reciprocal Lineweaver−Burk plot reported in supporting information (Fig. S11) confirmed the ATP-competitive mechanism of compound **1c**.

3.2.4. *Aβ42 self-aggregation*

Based on GSK-3β inhibitory activity, the most promising compounds, namely **1b**, **1c**, **3c**, and **4c**, were selected and evaluated for their ability to prevent $Aβ_{42}$ self-aggregation. Indeed, these derivatives are endowed with H-bond acceptor (HBA) and H-bond donor (HBD) groups that should enable them to establish hydrogen bonds with the Aβ peptide [40,41]. Furthermore, the aminopyrazole core has been reported to be able to significantly reduce the Aβ fibrilization process [38]. Screening was performed at a 1:1 ratio (50 μM) with $Aβ_{42}$, using a well-validated thioflavin T-based fluorescence assay [42,43] and using curcumin, a well-known antiaggregating agent, as a reference inhibitor. Despite the promising structural features, the selected derivatives showed a moderate antiaggregating profile, resulting in weaker inhibitors when compared to curcumin (inhibition = 79.9 %), with inhibition percentages ranging from 18.6 to 22.2, being **1c** the most active (Table S1). The very similar inhibition values displayed by this small set of compounds seemed to indicate a minor role for the flexibility of the spacer connecting the amide functions. Similarly, *p*-benzyl substituent does not seem to play a significant role in the inhibition of $Aβ_{42}$ aggregation for this class of derivatives [compare **1b** (21.0 %) with **1c** (22.2 %)]. However, the limited number of assayed compounds and the low activity towards amyloid aggregation do not allow to make any general SAR assumptions or more detailed comments.

3.2.5. *Metal chelating properties*

Imbalance in brain transition metals, including intraneuronal iron accumulation and extracellular copper and zinc pooling in amyloid plaques, is a commonly acknowledged characteristic of AD, despite disagreements among some [44]. Indeed, the levels of bivalent ions such

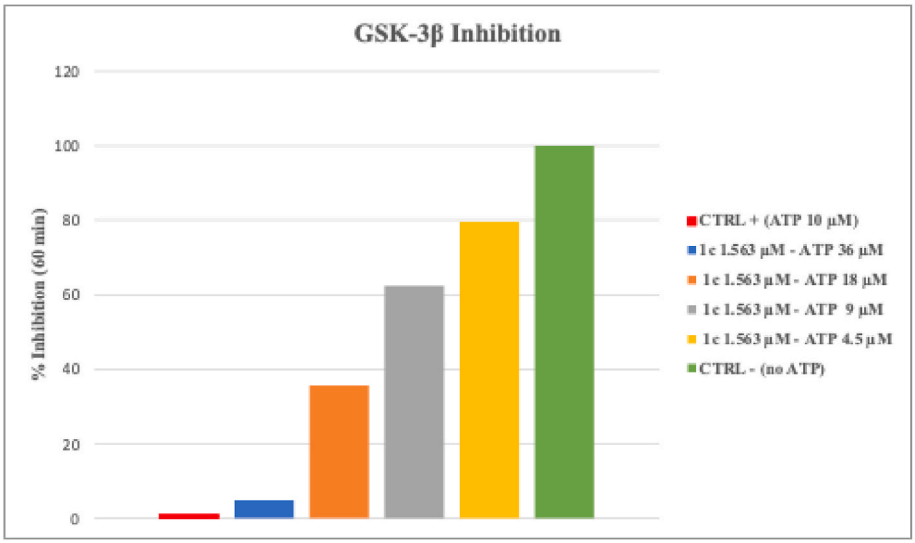

Fig. 5. Percentage of inhibition of GSK-3β at 60 min at different ATP concentrations. The positive control represents the enzymatic reaction in the previously defined conditions (ATP concentration equal to its K_M; SI, Fig. S4), while the negative control is without ATP to have the total inactivity of GSK-3β.

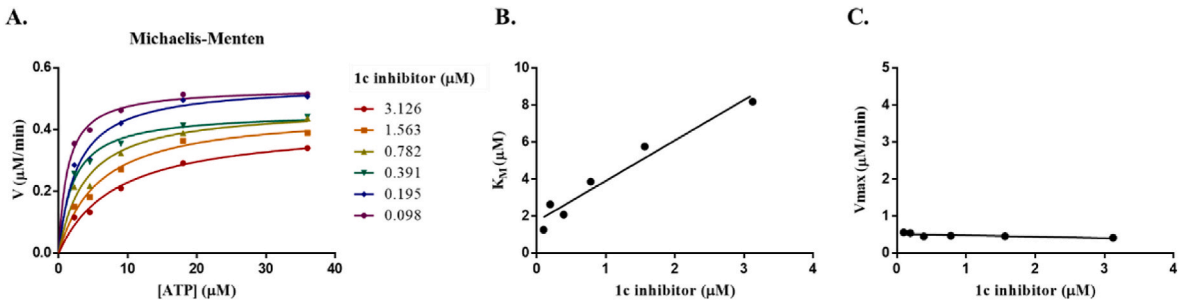

Fig. 6. **(A)** Reaction rates were determined by analysing GSK-3β activity over time and analyzed by linear regression analysis; **(B)** Plot of K_M against increasing concentrations of **1c**; **(C)** Plot of V_{max} against increasing concentrations of **1c**.

as copper, zinc, and iron appear to be from three to seven times higher in AD patients than in healthy individuals. Further, a correlation between metal dyshomeostasis and Aβ aggregation has been widely proven [14]. In particular, copper has been shown to exert a detrimental effect by hastening the formation of neurotoxic reactive oxygen species (ROS) and promoting Aβ neurotoxicity [45]. Notably, Cu-Aβ complex triggers the production of ROS, leading to oxidative damage, closely related to AD pathogenesis [46]. Hence, restoring metal homeostasis could prove beneficial in AD treatment.

Metal chelators capture metal ions and displace them from their target sites, thus intercepting their participation in redox processes and Aβ aggregation. Hence, to evaluate the chelating properties of the most promising compounds **1b**, **1c**, **3c**, and **4c** towards copper and zinc, UV–vis difference spectroscopy studies were performed. The chelating properties of the four selected compounds were preliminarily evaluated in methanol by recording their UV–vis spectra in the absence and presence of equimolar concentrations of Cu(II) and Zn(II). Two different behaviors were observed. For compounds **1b** and **1c**, which are characterized by the presence of a double bond in the spacer chain and *cis* isomerism, no spectral changes were observed upon the addition of copper or zinc, while for the more flexible derivatives **3c** and **4c**, a change in the absorption profile was detected. Indeed, the addition of Cu (II) to either **3c** or **4c** resulted in the appearance of a new band that partially overlapped with the original one (Fig. S12A and S12B). The difference spectrum, which was derived by sequentially subtracting the spectra of ligand (L) alone (either **3c** or **4c**) and metal (at the corresponding molar concentration) from the spectrum of the Cu(II):L complex, showed a positive band centered at 251 nm for **3c** and 254 nm for **4c**. For both compounds, an increase in the metal ion concentration resulted in a higher intensity of the difference absorption band as a consequence of a higher amount of complex formed (Fig. 7A and B). The observed changes in the absorbance spectra and the concentration-dependent trend support the chelating properties of **3c** and **4c** towards copper.

Similarly to what was observed for copper, upon adding equimolar concentrations of Zn(II) to **3c** and **4c**, the appearance of a shoulder was observed in the zero-order UV–vis spectra with resulting bands in the difference spectra centered at 246 nm and 247 nm for **3c** and **4c**, respectively (Fig. S13A and S13B). Note that the intensities of those bands were lower than those observed with Cu(II), likely because of a weaker chelating ability towards this bigger bivalent ion. Finally, in line with what was observed for Cu(II), no differences in the UV–vis spectra of **1b** and **1c** were observed when those compounds were mixed at equimolar concentration with a Zn(II) solution, indicating that those compounds were not able to form chelates with either metal ions.

The molar ratio method was applied to determine the stoichiometry

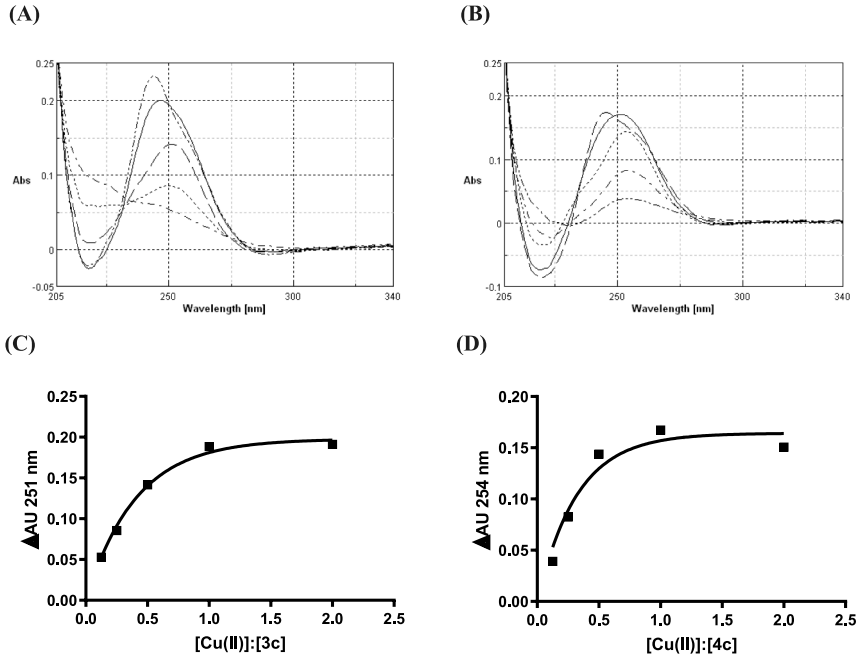

Fig. 7. Overlaid difference spectra for compounds **3c** (**A**) and **4c** (**B**) in the presence of increasing concentrations of Cu(II) (5–80 µM encompassing [Cu(II)]:[L] ratios from 0.125 to 2.0); increasing ΔAU values at the given wavelength as a function of the increased [Cu(II)]:[L] molar ratio for compounds **3c** (**C**) and **4c** (**D**).

of the [Cu(II)]:[L] complex for compounds **3c** and **4c**. However, while ΔAbs values were found to be dependent on the relative concentration of the metal:ligand ratio (Fig. 7A and B), at ratios close to or higher than 1.0 a shift in the maximum wavelength was observed, possibly indicating a different coordination mode occurring at the highest metal concentrations, hence, in the application of the molar ratio method for the assessment of the complex's stoichiometry, the ΔAU values at staring maxima, i.e. 251 nm and 254 nm for compounds **3c** (Fig. 7C) and **4c** (Fig. 7D), respectively, were considered. The observed trends let us hypothesize a complex's stoichiometry of 1:1; however, the shift of the λ_{max} at [M]:[L] higher than 1.0 let us also hypothesize that a different complexation stoichiometry may occur at higher molar ratios.

Concerning the investigations on Zn(II) complexation, a concentration-dependency was observed for both **3c** and **4c,** with no band shift for Zn(II):[L] molar ratios exceeding 1.0 (Fig. S13A and S13B, respectively). However, the lack of a clear saturation value in titration experiments, even when 2 equivalents of Zn(II) were added, prevented the assessment of the complex's stoichiometry. Finally, the chelation ability initially assessed in methanol was also confirmed in water (see Fig. S14A–D).

The chelating properties of **3c** and **4c** towards copper and zinc can then be seen as an added value from an anti-neurodegenerative perspective, in particular considering that Cu(II) appears as the more prone to act as central cationic metal in the formation of plaques and soluble oligomers. Restoring the intracellular copper homeostasis may decrease β-amyloid production, via different complex mechanisms. However, it must be always taken into consideration that metals also play an important physiological role in the CNS, and the role of copper has long been controversial [47–49]. Thus, while direct chelation therapy is still under debate, a modulation of copper levels, as in compounds **3c** and **4c**, may represent a valuable strategy to prevent metal-mediated ROS formation.

3.2.6. *Cytotoxicity*

The most promising compounds **1a-c**, **3c**, and **4c** were challenged in *per se* cytotoxicity experiments to determine the potential damage of their exposure to neuronal batches. In the SH-SY5Y neuroblastoma cell line, the incubation of the compounds at 2, 10 and 50 μM for 24 h induced no significant reduction in cell viability (MTT reduction assay, Fig. 8A).

For compounds **1c** and **4c**, selected for immunomodulation studies, a further CNS safety evaluation was performed on differentiated primary culture of cerebellar granule neurons (CGNs), due to the greater susceptibility of CGNs compared with other cell lines, including SH-SY5Y neuroblastoma cells. CGNs are the most numerous and pure neuronal population in the brain and can be easily isolated and cultured to recapitulate *in vitro* the neuronal development and maturation observed *in vivo*. Furthermore, CGNs, have been widely used to study molecular and biological processes of neuron physiology [50]. The selected compounds proved not to induce a significant reduction in cell viability when tested at 1, 5, 10, and 25 μM for 24 h (Fig. 8B).

Hence, the above pyrazole derivatives were shown to lack a toxic effect on neuronal cells at concentrations higher than the GSK-3β IC_{50} values.

3.2.7. *Immunomodulation studies*

Increasing evidence suggests that neuroinflammation plays a significant role in NDs, increasing the interest in the modulation of microglia phenotype [51]. Indeed, microglial cells represent the most important immune cells of the brain, becoming activated in neuropathological conditions, such as neurodegeneration. Activated microglia could polarize into M2 anti-inflammatory phenotype, typically at the initial stage of the pathology, with the aim to protect and repair neurons, or acquire a M1 pro-inflammatory phenotype, releasing inflammatory cytokines, finally leading to neuronal death. Then, the ability of microglial cells to shift from the neurotoxic M1 to the neuroprotective

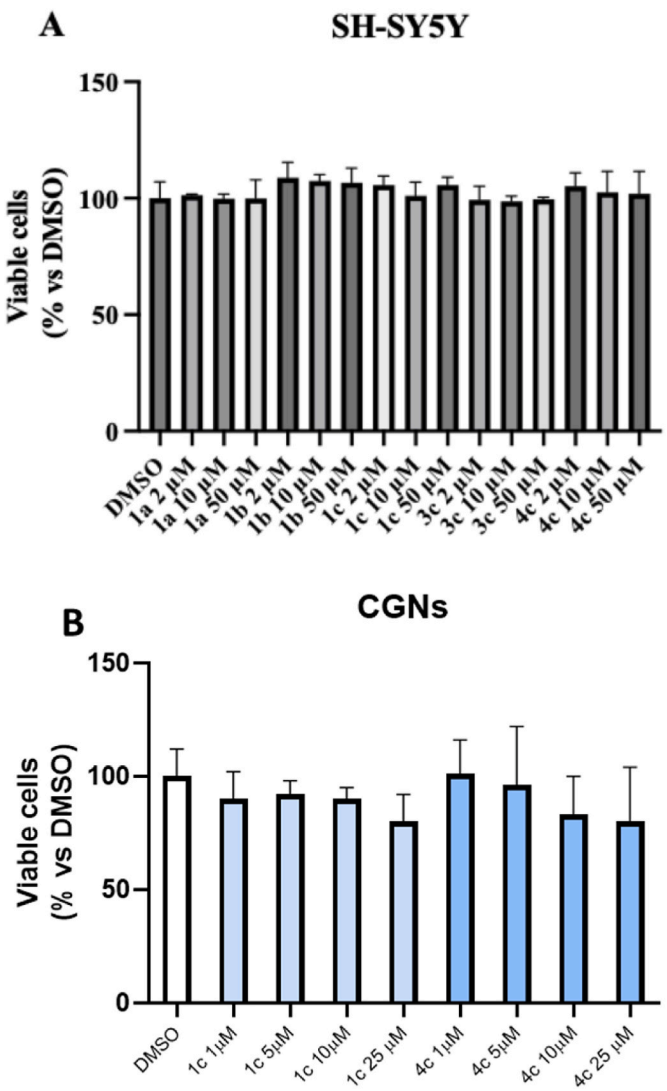

Fig. 8. Cytotoxicity assays were performed by measuring the mitochondrial NADPH oxidoreductase-dependent reduction of MTT to formazan in SH-SY5Y and CGNs cell lines. (**A**) SH-SY5Y cells were treated for 24 h with compounds **1a-c**, **3c**, and **4c** at 2, 10, and 50 μM, keeping the concentration of DMSO constant at 1 %. (**B**) Differentiated CGNs were treated with compounds **1c** and **4c** at increasing concentrations (1, 5, 10, and 25 μM) for 24 h in serum-free medium. Data are reported as mean ± SD of four independent experiments. One way-ANOVA, Dunnett's Multiple Comparison Test.

M2 phenotype and/or to reduce the extent of the injurious M1 phenotype is now widely considered a promising therapeutic strategy to tackle AD [52]. Compounds **1c** and **4c** were selected, considering their promising activity profiles, to evaluate their ability in reducing the activated state of microglia, thus exploiting immunomodulatory properties. N9 microglial cells were then pretreated (2 h) with **1c** and **4c** (5 and 10 μM), followed by 24 h stimulation with LPS 100 ng/mL. Microglial phenotype was evaluated by the western blot analysis of the levels of pro-inflammatory iNOS (inducible Nitric Oxide Synthase, M1 marker) which responds to LPS stimulation [53] and of the Triggering Receptor Expressed on Myeloid cells 2 (TREM2), a M2 marker [54]. As reported in Fig. 9, both compounds were able to reduce the inflammatory activation of N9 cells induced by LPS treatment, as demonstrated by the significative and dose-dependent reduction of iNOS expression in response to 10 μM treatment (Fig. 9A–D, and 9B, E). However, the phagocytic properties of microglia were preserved especially in response to treatment with compound **1c** as demonstrated by the slight increase

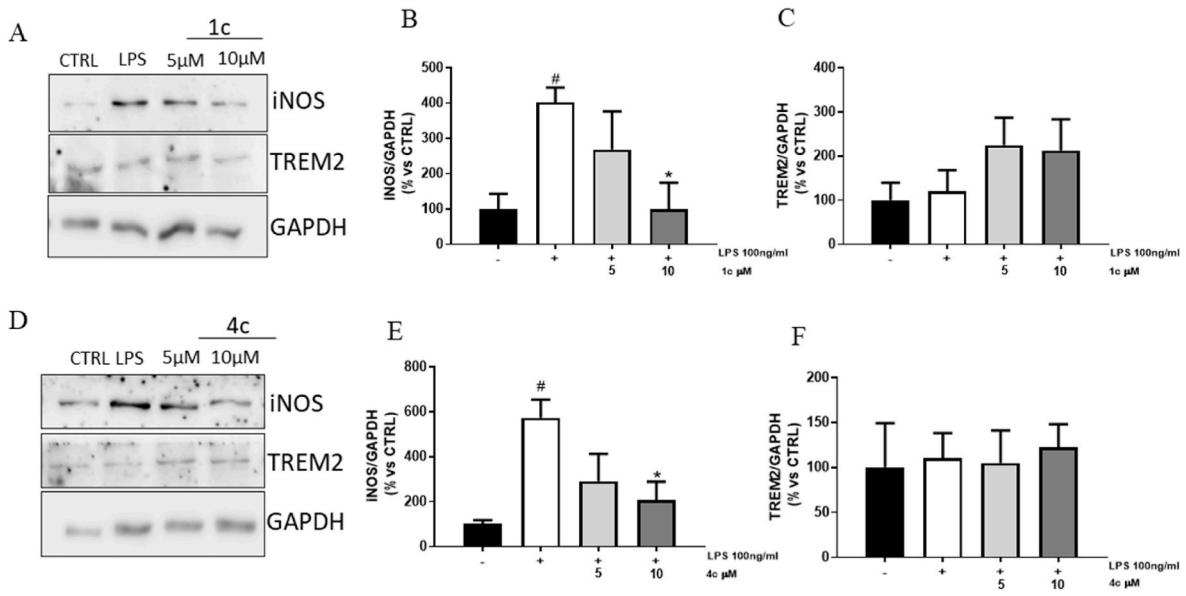

Fig. 9. Immunomodulatory effects of **1c** and **4c** on microglial cells. Representative western blot analysis of iNOS and TREM2 expression in N9 cells pre-treated (2 h) with **1c** (**A**) and **4c** (**D**) and subsequently activated with LPS (100 ng/ml) for 24 h. Densitometric analysis of iNOS (**B**, **E**) and TREM2 (**C**, **F**) expression respectively for **1c** and **4c** treatment. GAPDH was used as loading control. Densitometric results are expressed as percentage *vs* CTRL are the mean ± SE of three independent experiments. One way-ANOVA, Dunnett's Multiple Comparison Test. #p < 0,05 *vs* CTRL. *p < 0,05 vs LPS.

in TREM2 expression (Fig. 9C–F), a critical factor in the regulation of immune surveillance. Indeed, TREM2 is required for the conversion of microglia from a homeostatic to a disease activated state which potentially confers neuroprotection by enhancing microglial function, including an upregulation of genes implicated in migration, phagocytosis, survival and lipid metabolism [54,55]. In this perspective, compound **1c**, at 10 μM, appeared to effectively promote the neuroprotective function of microglial cells by significantly reducing the pro-inflammatory signature and enhancing phagocytosis.

3.2.8. Parallel artificial membrane permeability assay - blood-brain barrier

The main obstacle to effective treatment in CNS diseases is the ability of drugs to cross the blood-brain barrier (BBB) and reach their therapeutic targets at suitable concentrations. Since most CNS drugs pass through the BBB by transcellular passive diffusion, the modified Parallel Artificial Membrane Permeability Assay (PAMPA) with porcine brain lipids is often used in the early stage of drug discovery campaigns as a high-throughput and cost-effective method for predicting BBB permeability controlled by passive transport [56].

Therefore, the most promising compounds **1c** and **4c** were tested for their ability to permeate the BBB. To validate assay conditions, piroxicam, caffeine, the highly permeable drug propranolol and the poorly permeable drug furosemide were also evaluated [56–58]. Based on the results reported in Table 3, both derivatives displayed good CNS permeability, with apparent permeability values (P_{app}) of (2.63 ± 0.04 and 2.30 ± 0.03) × 10^{-6} cm/s, respectively, higher than caffeine and piroxicam.

Table 3
Permeability results from the PAMPA−BBB.

	PAMPA-BBB P_{app} (10^{-6} cm/s)	$LogP_{app}$
Furosemide	*u.d.l.*[a]	–
Caffeine[b]	1.153 ± 0.030	−5.94 ± 0.01
Piroxicam[c]	1.040 ± 0.115	−5.98 ± 0.05
Propranolol	6.180 ± 0.346	−5.21 ± 0.02
1c	2.630 ± 0.042	−5.59 ± 0.01
4c	2.301 ± 0.035	−5.64 ± 0.06

[a] u.d.l. under the detection limit.
[b] Literature value P_{app} 1.6 × 10^{-6} cm/s [56].
[c] Literature value P_{app} 0.9 × 10^{-6} cm/s [56]. Data are the mean ± SD of two independent experiments.

4. Discussion and conclusions

AD is recognized as a multifactorial neurodegenerative disorder with several processes contributing to the disease's onset and progression. Thus, a polypharmacological approach aimed at targeting different important pathogenetic factors is a modern promising strategy for AD, although the development of multi-target inhibitors is highly challenging. In light of this, in this paper we exploited acylaminopyrazole as privileged structure to develop compounds able to act at validated targets in a polypharmacological perspective for AD.

Firstly, we focused our attention on GSK-3β inhibition, due to the recognized role of this kinase as a linker between amyloid and tau cascades and its up-regulation in the brains of AD patients. A series of acylated aminopyrazole derivatives bearing a *N*-methylbenzyl terminal moiety was prepared, and two rounds of optimization led to derivatives **1b**, **1c**, **3c**, and **4c**, with IC_{50} values in the low micromolar range. In this respect, it is essential to highlight that a fine tuning of the inhibition of GSK-3β, capable of restoring physiological activity levels but preserving its key biological role, is nowadays considered more desirable to obtain a significant therapeutic effect. Indeed, due to the essential role played by this kinase, responsible for the regulation of glycogen metabolism and involved in different cellular processes such as cell cycle progression, cell proliferation, and inflammation, the appropriate modulation of its function, rather than its complete inhibition, could avoid the occurrence of unacceptable side effects [59]. In addition, for this class of compounds, structure-activity relationships were defined and, taking advantage of Microfluidic Mobility Shift Assay (MMSA), their mechanism of action was established.

Then, in a multifunctional perspective, the most promising derivatives were evaluated in other relevant AD pathological processes. In particular, based on previous evidence [9,10], the new derivatives, featuring a pyrazole core linked to an amide moiety, were speculated to be able to provide a favourable hydrogen bonding network for interaction with Aβ fragments, reducing their propensity to aggregate. Unfortunately, despite the premises, the tested compounds only showed a fair antiaggregating profile, with inhibition percentages ranging from 18.6

to 22.2 %, with the best results for **1c**. Considering the low number of compounds tested, clear structure-activity relationships could not be established, but it can be inferred that the bulky terminal *N*-methylamide function could prevent an effective fitting with Aβ oligomers.

Then, as the acylaminopyrazoles derivatives could form coordination bonds, their chelating activity was assessed. Indeed, dysregulation of homeostasis of metals has been related to the pathogenesis of AD, and metal chelation therapy has been proposed to be a promising approach in restoring metal balance and reducing neurotoxicity. Chelating properties of compounds **1b**, **1c**, **3c**, and **4c** towards copper and zinc were evaluated. No activity was observed for the rigid derivatives **1b** and **1c**, bearing a double bond in the spacer chain. On the other hand, analogues **3c** and **4c**, with no conformational restriction, showed interesting chelating properties towards both copper and zinc ions. Indeed, the higher flexibility of the alkyl spacer could probably allow the dicarbonyl chains of **3c** and **4c** to adopt a more suitable conformation for metal coordination, almost certainly prevented by the presence of the double bond in **1b** and **1c**.

Taken together, these results prompted us to select compounds **1c** and **4c** for futher studies.

Toxicity of drug candidates after chronic treatment is an important issue in AD drug discovery approaches. In consideration of this, cytotoxicity in neuroblastoma cell line and on a differentiated primary culture of cerebellar granule neurons was first assessed, and the tested compounds were found not to reduce the number of metabolic active cells in comparison to the vehicle.

Then, functional studies were performed, and compounds **1c** and **4c** were evaluated for their immunomodulatory properties, through their ability to reduce the activated state of microglia. The results proved that both compounds were able to reduce the inflammatory activation induced on microglial cells by LPS stimulation, showing a significative and dose-dependent reduction of iNOS expression. Finally, as the ability of drugs to cross the blood-brain barrier (BBB) is one of the main obstacles to effective treatment in CNS diseases, the PAMPA test for compounds **1c** and **4c** was performed to predict BBB permeability. Both compounds showed good apparent permeability values and might be suitable for central nervous system studies.

Taken together, although very preliminary, these results pointed out that the acylaminopyrazole scaffold could represent a valuable privileged structure to be exploited for the design of multifunctional compounds, effective at cellular level, as potential new disease-modifying agents to treat AD. A forthcoming medicinal chemistry campaign will be directed towards the optimization of the benzylamide side chain to improve activity on the selected targets.

5. Experimental section

5.1. Chemistry

General Methods. All chemicals were purchased from Aldrich Chemistry, Milan (Italy), or Alfa Aesar, Milan (Italy), and were of the highest purity. The selected solvents were of analytical grade. Thin layer chromatography (TLC) on precoated silica gel plates (Merck Silica Gel 60 F254) was applied to monitor reaction progress, and then visualized with a UV254 lamplight. Compounds purifications were performed by flash chromatography on silica gel columns (Kieselgel 40, 0.040–0.063 mm, Merck). ^{1}H NMR spectra for the intermediate compounds were recorded on a Varian Gemini spectrometer working at 400 MHz, while for the final compounds ^{1}H NMR and ^{13}C NMR spectra were recorded on a Bruker spectrometer working at 600 MHz and at 150 MHz, respectively, in DMSO-d_6 solutions unless otherwise indicated. Chemical shifts (δ) were reported as parts per million (ppm) values relative to tetramethylsilane (TMS) as internal standard; coupling constants (J) are reported in Hertz (Hz). Standard abbreviations were used for indicating spin multiplicities: s (singlet), d (doublet), dd (double doublet), t (triplet), br (broad), q (quartet) or m (multiplet). UHPLC−MS analyses were run on a Waters ACQUITY ARC UHPLC/MS system, consisting of a QDa mass spectrometer equipped with an electrospray ionization interface and a 2489 UV/Vis detector at wavelengths (λ) 254 nm and 365 nm. The analyses were performed on an XBridge BEH C18 column (10 × 2.1 mm i.d., particle size 2.5 μm) with a XBridge BEH C18 VanGuard Cartridge precolumn (5 mm × 2.1 mm i.d., particle size 1.8 μm), with mobile phases consisting in H_2O (0.1 % formic acid) (A) and MeCN (0.1 % formic acid) (B). Electrospray (ES) ionization in positive and negative modes was applied in the mass scan range of 50–1200 Da. Method and gradients used were the following: Generic method. Linear gradient: 0−0.78 min, 20 % B; 0.78–2.87 min, 20−95 % B; 2.87–3.54 min, 95 % B; 3.54–3.65 min, 95-20 % B; 3.65-5-73, 20 % B. Flow rate: 0.8 mL/min. All tested compounds were found to have >95 % purity. Compounds were named relying on the naming algorithm developed by CambridgeSoft Corporation and used in ChemBioDraw Ultra (version 23.0).

5.1.1. General procedure a for the preparation of (Z)-4-(benzylmethylamino)-4-oxobutenoic acid (7a-m), 4-(benzylmethylamino)-4-oxobutanoic acid (8a-c), 5-(benzylmethylamino)-5-oxopentanoic acid (9a-c)

The appropriate anhydride (1.2 eq) was added at a solution of the opportune methylbenzaldehyde (1 eq) and triethylamine (3eq) in DCM, then the mixture was stirred overnight at rt. After the night the reaction was diluted with DCM and washed twice with HCl 3 M, and the organic phase was concentrated under vacuum.

5.1.2. (Z)-4-(benzyl(methyl)amino)-4-oxobut-2-enoic acid (7a)

Using the procedure A, starting from the commercial *N*-benzylmethylamine **6a** (0.26 mL, 2.0 mmol) and maleic anhydride (0.227 g, 2.3 mmol), 0.220 g of pink oil was obtained (50 %). ^{1}H NMR (400 MHz, $CDCl_3$) δ 3.11 (s, 3H, CH_3), 4.69 (s, 2H, CH_2Ph), 6.42 (d, J = 12.9 Hz, 1H, CH=C), 6.71 (d, J = 12.9 Hz, 1H, CH=C), 7.15–7.20 (m, 2H, Ar), 7.32–7.47 (m, 3H, Ar), 15.53 (s, 1H, OH).

5.1.3. (Z)-4-((4-methoxybenzyl)(methyl)amino)-4-oxobut-2-enoic acid (7b)

Using the procedure A, starting from **6b** [15] (0.242 g, 2.5 mmol) and maleic anhydride (0.250 g, 2.1 mmol), 0.250 g of pink oil was obtained (49 %). ^{1}H NMR (400 MHz, $CDCl_3$) δ 3.10 (s, 3H, NCH_3), 3.82 (s, 3H, OCH_3), 4.63 (s, 2H, CH_2Ph), 6.44 (d, J = 13.2 Hz, 1H, CH=C), 6.68 (d, J = 14.8 Hz, 1H, CH=C), 6.89 (d, J = 8.8 Hz, 2H, Ar), 7.22 (d, J = 8.8 Hz, 2H, Ar), 15.54 (s, 1H, OH).

5.1.4. (Z)-4-((4-chlorobenzyl)(methyl)amino)-4-oxobut-2-enoic acid (7c)

Using the procedure B, starting from **6c** [15] (0.300 g, 1.9 mmol) and maleic anhydride (0.227 g, 2.3 mmol), 0.400 g of pink oil was obtained (82 %). ^{1}H NMR (400 MHz, $CDCl_3$) δ 3.13 (s, 3H, NCH_3), 4.67 (s, 2H, CH_2Ph), 6.40 (d, J = 12.9 Hz, 1H, CH=C), 6.69 (d, J = 12.9 Hz, 1H, CH=C), 7.27 (d, J = 8.4 Hz, 2H, Ar), 7.41 (d, J = 8.8 Hz, 2H, Ar), 15.62 (s, 1H, OH).

5.1.5. 4-(benzyl(methyl)amino)-4-oxobutanoic acid (8a)

Using procedure A, starting from the commercial *N*-benzylmethylamine **6a** (0.32 mL, 2.5 mmol) and succinic anhydride (0.300 g, 3.0 mmol), a light brown oil was obtained (88 %). ^{1}H NMR (400 MHz, $CDCl_3$) δ 2.68–2.77 (m, 4H, CH_2), 2.96 (s, 3H, NCH_3), 4.57 (s, 2H, CH_2Ph), 7.15–7.20 (m, 2H, Ar), 7.32–7.47 (m, 3H, Ar), 11.81 (s, 1H, OH).

5.1.6. 4-((4-methoxybenzyl)(methyl)amino)-4-oxobutanoic acid (8b)

Using procedure A, starting from **6b** [15] (0.300 g, 2.0 mmol) and succinic anhydride (0.239 g, 2.4 mmol), a yellow oil was obtained (98 %). ^{1}H NMR (400 MHz, $CDCl_3$) δ 2.70–2.77 (m, 4H, CH_2), 2.93 (s, 3H, NCH_3), 3.81 (s, 3H, OCH_3), 4.54 (s, 2H, CH_2Ph), 6.86 (d, J = 8.8 Hz, 2H, Ar), 7.17 (d, J = 8.8 Hz, 2H, Ar), 11.80 (s, 1H, OH).

5.1.7. 4-((4-chlorobenzyl)(methyl)amino)-4-oxobutanoic acid (8c)

Using procedure A, starting **6c** [15](0.246 g, 1.6 mmol) and succinic anhydride (0.190 g, 1.9 mmol), a white solid was obtained (89 %). ^{1}H NMR (400 MHz, $CDCl_3$) δ 2.68–2.77 (m, 4H, CH_2), 2.96 (s, 3H, NCH_3), 4.57 (s, 2H, CH_2Ph), 7.17 (d, $J = 8.0$ Hz, 2H, Ar), 7.29 (d, $J = 8.4$ Hz, 2H, Ar), 11.81 (s, 1H, OH).

5.1.8. 5-(benzyl(methyl)amino)-5-oxopentanoic acid (9a)

Using procedure A, starting from the commercial *N*-benzylmethylamine **6a** (0.32 mL, 2.5 mmol) and glutaric anhydride (0.342 g, 3.0 mmol), a yellow oil was obtained (44 %). ^{1}H NMR (400 MHz, $CDCl_3$) δ 2.02 (q, $J = 7.2$ Hz, 2H, CH_2), 2.49 (t, $J = 7.2$ Hz, 4H, CH_2CO), 2.92 (s, 3H, NCH_3), 4.60 (s, 2H, CH_2Ph), 7.21–7.25 (m, 2H, Ar), 7.28–2.40 (m, 3H, Ar), 12.01 (s, 1H, OH).

5.1.9. 5-((4-methoxybenzyl)(methyl)amino)-5-oxopentanoic acid (9b)

Using procedure A, starting from **6b** [15] (0.300 g, 2.0 mmol) and glutaric anhydride (0.273 g, 2.4 mmol), 0.231 g of a yellow oil was obtained (53 %). ^{1}H NMR (400 MHz, $CDCl_3$) δ 2.02–2.03 (m, 2H, CH_2), 2.43–2.52 (m, 4H, CH_2CO), 2.90 (s, 3H, NCH_3), 3.81 (s, 3H, OCH_3), 4.52 (s, 2H, CH_2Ph), 7.07 (d, $J = 8.4$ Hz, 2H, Ar), 7.17 (d, $J = 8.8$ Hz, 2H, Ar), 11.99 (s, 1H, OH).

5.1.10. 5-((4-chlorobenzyl)(methyl)amino)-5-oxopentanoic acid (9c)

Using procedure A, starting **6c** [15] (0.300 g, 1.9 mmol) and glutaric anhydride (0.264 g, 2.3 mmol), 0.260 g of a yellow oil was obtained (53 %). ^{1}H NMR (400 MHz, $CDCl_3$) δ 2.01–2.03 (m, 2H, CH_2), 2.43–2.50 (m, 4H, CH_2CO), 2.94 (s, 3H, NCH_3), 4.55 (s, 2H, CH_2Ph), 7.08 (d, $J = 8.4$ Hz, 2H, Ar), 7.17 (d, $J = 8.4$ Hz, 2H, Ar), 12.03 (s, 1H, OH).

5.1.11. General procedure B for the preparation of (E)-4-(benzylmethylamino)-4-oxobutenoic acid (10a-c)

The appropriate *N*-benzyl-*N*-methylamine (1 eq) was added dropwise at a solution of fumaric acid (3 eq), HATU (1 eq) and DIPEA (2 eq) in DMF. The mixture was stirred at rt for 2 h, then it was quenched in water and extracted with EA and the organic phase was evaporated under vacuum. The product was purified with a flash column chromatography.

5.1.12. (E)-4-(benzyl(methyl)amino)-4-oxobut-2-enoic acid (10a)

Using procedure B, starting from the commercial *N*-benzyl-*N*-methylamine **6a** (0.26 ml, 2 mmol) and fumaric acid (0.696 g, 6 mmol), **10a** was obtained, purified with column chromatography. A white oil was obtained (56 %). ^{1}H NMR (400 MHz) δ 3.01 (s, 3H, NCH_3), 4.57 (s, 2H, CH_2Ph), 6.55 (d, $J = 15.2$ Hz, 1H, CH=C), 7.21–7.25 (m, 2H, Ar), 7.33–7.39 (m, 4H, Ar and CH=C), 15.43 (s, 1H, OH).

5.1.13. (E)-4-((4-methoxybenzyl)(methyl)amino)-4-oxobut-2-enoic acid (10b)

Using procedure B, starting from **6b** [15] (0.300 g, 2 mmol) and fumaric acid (0.689 g, 6 mmol), an oil was obtained (77 %). ^{1}H NMR (400 MHz) δ 3.01 (s, 3H, NCH_3), 3.81 (s, 3H, OCH_3), 4.55 (s, 2H, CH_2Ph), 6.55 (d, $J = 15.2$ Hz, 1H, CH=C), 7.07 (d, $J = 8.4$ Hz, 2H, Ar), 7.30–7.35 (m, 3H, Ar and CH=C), 15.40 (s, 1H, OH).

5.1.14. (E)-4-((4-chlorobenzyl)(methyl)amino)-4-oxobut-2-enoic acid (10c)

Using procedure B, starting from **6c** [15] (0.300 g, 1.9 mmol) and fumaric acid (0.672 g, 5.8 mmol **10c** was obtained without other purification in quantitative yield. ^{1}H NMR (400 MHz) δ 3.01 (s, 3H, NCH_3), 4.55 (s, 2H, CH_2Ph), 6.55 (d, $J = 15.2$ Hz, 1H, CH=C), 7.33–7.39 (m, 3H, Ar and CH=C), 7.49 (d, $J = 8.6$ Hz, 2H, Ar), 15.47 (s, 1H, OH).

5.1.15. General procedure C for the preparation of N,N-benzylmethylamino oxoacetic acid derivatives (11a-c)

A solution of ethyl 2-chloro-2-oxyacetate (1.3 eq) in DCM was added at a mixture of the appropriate *N,N*-benzyl-methylamine (1 eq) and DIPEA (3 eq) in DCM. The reaction was stirred at rt for 3.5 h and then it was washed twice with water and twice with saturated solution of $NaHCO_3$ and the organic phase was evaporated under vacuum. Then the crude was solubilized into a mixture of THF/H_2O (1:1) and lithium hydroxide (1.1 eq) was added; the reaction stirred at rt for 6 h. At the end the mixture was concentrated under vacuum to remove the organic phase, and the aqueous phase was acidified at pH = 5 with HCl 0.5 M, and then this phase was concentrated under vacuum.

5.1.16. 2-(benzyl(methyl)amino)-2-oxoacetic acid (11a)

Using procedure C, starting from the commercial *N*-benzyl-*N*-methylamine **6a** (0.300 g, 2.5 mmol) and ethyl 2-chloro-2-oxyacetate (0.36 mL, 3.2 mmol), a white solid was obtained (92 %). ^{1}H NMR (400 MHz) δ 2.78 (s, 3H, NCH_3), 4.41 (s, 2H, CH_2Ph), 7.20 (d, $J = 7.2$ Hz, 2H, Ar), 7.30–7.34 (m, 1H, Ar), 7.40 (d, $J = 6.8$ Hz, 2H, Ar), 11.85 (s, 1H, OH).

5.1.17. 2-((4-methoxybenzyl)(methyl)amino)-2-oxoacetic acid (11b)

Using procedure C, starting from **6b** [15] (0.190 g, 1.6 mmol) and ethyl 2-chloro-2-oxyacetate (0.22 mL, 2.0 mmol) a white solid was obtained (88 %). ^{1}H NMR (400 MHz, $CDCl_3$) δ 2.88 (s, 3H, NCH_3), 3.81 (s, 3H, OCH_3), 4.38 (s, 2H, CH_2Ph), 6.89 (d, $J = 8.8$ Hz, 2H, Ar), 7.22 (d, $J = 8.8$ Hz, 2H, Ar), 11.92 (s, 1H, OH).

5.1.18. 2-((4-chlorobenzyl)(methyl)amino)-2-oxoacetic acid (11c)

Using procedure C, starting from **6c** [15] (0.200 g, 1.3 mmol) and ethyl 2-chloro-2-oxyacetate (0.19 mL, 1.7 mmol), a white solid was obtained (97 %). ^{1}H NMR (400 MHz, $CDCl_3$) δ 7.17 (d, $J = 8.4$ Hz, 2H, Ar), 7.08 (d, $J = 8.4$ Hz, 2H, Ar), 4.44 (s, 2H, CH_2Ph), 2.90 (s, 3H, NCH_3), 11.89 (s, 1H, OH).

5.1.19. (Z)-4-((5-methyl-1H-pyrazol-3-yl)amino)-4-oxobut-2-enoic acid (12)

A solution of 3-amino-5-methylpyrazole (0.600 g, 1 eq), maleic anhydride (0.733 g, 1.2 eq) and triethylamine (2.58 ml, 3 eq) in DCM was stirred at rt for 1 h. The solid formed from the reaction was filtered and washed with DCM. 1.076 g of pink solid was obtained without other purification (89 %). ^{1}H NMR (400 MHz) δ 2.20 (s, 3H, CH_3-pyrazole), 6.09 (s, 1H, CH-pyrazole), 6.32 (d, $J = 2.8$ Hz, 1H, CH=C), 6.45 (d, $J = 12.0$ Hz, 1H, CH=C), 11.02 (s, 1H, NHCO), 11.55 (s, 1H, NH-pyrazole), 13.65 (s, 1H, OH).

5.1.20. General procedure D for the preparation of final compounds 1a-m, 2a-c, 3a-c, 4a-c, 5a-c

A mixture of opportune acid (1.2 eq), opportune amine (1 eq), HATU (1 eq) and DIPEA (2.5 eq) was stirred in DMF for 4 h at rt. Then the reaction was quenched in water. If a solid has been formed, it was filtered to obtain the desired compound, otherwise the solution was extracted with ethyl acetate and washed with brine and $NaHCO_3$ saturated solution, the organic phase was concentrated under vacuum and the solid was purified with a column chromatography.

5.1.21. N^1-benzyl-N^1-methyl-N^4-(5-methyl-1H-pyrazol-3-yl)maleamide (1a)

Using procedure D, starting from 3-amino-5-methylpyrazole (0.080 g, 0.83 mmol) and **7a** (0.220 g, 1.00 mmol), 0.160 g of white solid was obtained, with a purification with column chromatography (DCM/MeOH (NH_4OH 5 %) 9:1) (65 %). ^{1}H NMR (600 MHz): δ 2.21 (s, 3H, CH_3-pyrazole), 2.77 (d, 3H, $J = 23.6$ Hz, NCH_3), 4.50 (d, 2H, $J = 76.4$ Hz, CH_2Ph), 6.26 (dd, 1H, $J = 11.9$ and 3.6 Hz, C=CH), 6.35 (s, 1H, CH-pyrazole), 6.58 (dd, 1H, $J = 23.1$ and 11.8 Hz, C=CH), 7.22–7.30 (m, 2H, Ar), 7.31–7.36 (m, 2H, Ar), 7.40 (d, 1H, $J = 6.8$ Hz, Ar), 10.62 (1H, d, $J = 6.0$ Hz, NH), 12.06 (s, 1H, NH-pyrazole). ^{13}C NMR: δ 10.70 (1C, CH_3-pyrazole), 31.34, 34.68 (1C, NCH_3), 48.82, 53.19 (1C, $\underline{CH_2}Ph$), 95.69 (1C, CH-pyrazole), 125.09 (1C), 125.77 (1C), 126.98 (1C), 127.48

(1C), 127.75 (1C), 128.35 (1C), 128.57 (1C), 135.35 (1C), 136.98 (1C), 137.34 (1C), 161.15 (1C, C=O), 167.91 (1C, C=O). MS (ES) *m/z*: 299.35 (M + H).

5.1.22. N^1-(4-methoxybenzyl)-N^1-methyl-N^4-(5-methyl-1H-pyrazol-3-yl) maleamide (1b)

Using procedure D, starting from 3-amino-5-methylpyrazole (0.081 g, 0.84 mmol) and **7b**, 0.180 g of yellow solid was obtained, with a purification with column chromatography (EA/MeOH (NH_4OH 5 %) 9.75:0.25) (65.5 %). ^{1}H NMR (600 MHz): δ 2.20 (s, 3H, CH_3-pyrazole), 2.73 (d, 3H, J = 19.4, NCH_3), 3.73 (d, 3H, J = 10.05 Hz, OCH_3), 4.42 (d, 2H, J = 78.0 Hz, CH_2Ph), 6.25 (dd, 1H, J = 11.9 and 8.5 Hz, C=CH), 6.34 (s, 1H, CH-pyrazole), 6.57 (dd, 1H, J = 44.2and 11.9 Hz, C=CH), 6.89 (t, 2H, J = 8.4 Hz, Ar), 7.21 (d, 1H, J = 8.6 Hz, Ar), 7.31 (d, 1H, J = 8.6 Hz, Ar), 10.62 (s, 1H, NH), 12.05 (s, 1H, NH-pyrazole). ^{13}C NMR: δ 10.68 (1C, CH_3-pyrazole), 31.04, 34.39 (1C, NCH_3), 48.12, 55.05 (1C, CH_2Ph), 55.05 (1C, OCH_3), 95.70 (CH-pyrazole), 113.74 (1C, Ar), 113.93 (1C, Ar), 125.03 (1C), 125.65 (1C), 128.73 (1C), 128.90 (1C), 129.20 (1C), 135.34 (1C), 138.31 (1C), 147.14 (1C), 158.38 (1C), 161.12 (1C, C=O), 167.71 (1C, C=O). MS (ES) *m/z*: 329.37 (M + H).

5.1.23. N^1-(4-chlorobenzyl)-N^1-methyl-N^4-(5-methyl-1H-pyrazol-3-yl) maleamide (1c)

Using procedure D, starting from 3-amino-5-methylpyrazole (0.064 g, 0.66 mmol) and **7c** (0.076 g, 0.79 mmol), 0.160 g of white solid was obtained, with a purification with column chromatography (DCM/MeOH (NH_4OH 5 %) 9.75:0.25) (73 %). ^{1}H NMR (600 MHz): δ 2.21 (s, 3H, CH_3-pyrazole), 2.76 (d, 3H, J = 25.7, NCH_3), 4.49 (d, 2H, J = 73.3 Hz, CH_2Ph), 6.26 (dd, 1H, J = 11.9 and 8.9 Hz, C=CH), 6.35 (s, 1H, CH-pyrazole), 6.57 (dd, 1H, J = 22.2and 11.8 Hz, C=CH), 7.32 (d, 1H, J = 8.5 Hz, Ar), 7.36–7.42 (m, 2H, Ar), 7.45 (d, 1H, J = 8.5 Hz, Ar), 10.62 (d, 1H, J = 10.6 Hz, NH), 12.05 (s, 1H, NH-pyrazole). ^{13}C NMR: δ 10.67 (1C, CH_3-pyrazole), 31.31, 34.68 (1C, NCH_3), 48.19, 52.48 (1C, CH_2Ph), 95.68 (CH-pyrazole), 125.12 (1C), 125.76 (1C), 128.23 (1C), 128.46 (1C), 129.41 (1C), 129.66 (1C), 131.55 (1C), 135.24 (1C), 136.43 (1C), 138.31 (1C), 147.12 (1C), 161.10 (1C, C=O), 168.00 (1C, C=O). MS (ES) *m/z*: 333.79 (M + H).

5.1.24. N^1-methyl-N^4-(5-methyl-1H-pyrazol-3-yl)-N^1-(4-nitrobenzyl) maleamide (1d)

Using procedure D, starting from **6d** [15] (0.166 g, 1.00 mmol) and **12** (0.234 g, 1.2 mmol), 0.150 g of a white solid was obtained, with a purification with column chromatography (DCM/MeOH (NH_4OH 5 %) 9.5:0.5) (44 %). ^{1}H NMR (600 MHz): δ 2.21 (d, 3H, J = 5.7 Hz, CH_3-pyrazole), 2.82 (d, 3H, J = 25.2 Hz, NCH_3), 4.65 (d, 2H, J = 65.8 Hz, CH_2Ph), 6.27 (dd, 1H, J = 30.4 and 11.9 Hz, C=CH), 6.36 (d, 1H, J = 12.1 Hz, CH-pyrazole), 6.58 (d, 1H, J = 11.7 Hz, C=CH), 7.54–7.77 (m, 2H, Ar), 8.12–8.25 (m, 2H, Ar), 10.63 (d, 1H, J = 35.2 Hz, NH), 12.07 (s, 1H, NH-pyrazole). ^{13}C NMR: δ 10.67 (1C, CH_3-pyrazole), 31.76, 35.03 (1C, NCH_3), 48.65, 52.73 (1C, CH_2Ph), 95.68 (1C, CH-pyrazole), 123.39 (1C), 125.27 (1C), 128.77 (1C), 135.14 (1C), 138.33 (1C), 145.25 (1C), 145.73 (1C), 146.63 (1C), 146.77 (1C), 147.11 (1C), 161.12 (1C, C=O), 168.26 (1C, C=O). MS (ES) *m/z*: 344.34 (M + H).

5.1.25. N^1-(4-cyanobenzyl)-N^1-methyl-N^4-(5-methyl-1H-pyrazol-3-yl) maleamide (1e)

Using procedure D, starting from **6e** [16] (0.400 g, 2.74 mmol) and **12** (0.641 g, 3.29 mmol 0.150 g of a white solid was obtained, with a purification with column chromatography (DCM/MeOH (NH_4OH 5 %) 9.5:0.5) (17 %). ^{1}H NMR (600 MHz): δ 2.21 (d, 1H, J = 6.9 Hz, CH_3-pyrazole), 2.80 (d, 3H, J = 32.4 Hz, NCH_3), 4.60 (d, 2H, J = 68.6 Hz, CH_2Ph), 6.26 (dd, 1H, J = 27.0 and 11.8 Hz, C=CH), 6.35 (d, 1H, J = 14.6 Hz, CH-pyrazole), 6.57 (d, 1H, J = 11.8 Hz, C=CH), 7.57 (dd, 2H, J = 87.6and 8.2 Hz, Ar), 7.81 (dd, 2H, J = 16.5and 8.4 Hz, Ar), 10.63 (d, 1H, J = 29.0 Hz, NH), 12.06 (s, 1H, NH-pyrazole). ^{13}C NMR: δ 10.71 (1C, CH_3-pyrazole), 31.67, 35.02 (1C, NCH_3), 48.85, 52.96 (1C, CH_2Ph), 95.73 (CH-pyrazole), 109.74 (1C), 110.12 (1C), 118.79 (1C), 118.99 (1C), 125.23 (1C), 128.54 (1C), 132.27 (1C), 132.47 (1C), 135.23 (1C), 143.08 (1C), 143.51 (1C), 161.14 (1C, C=O), 168.28 (1C, C=O). MS (ES) *m/z*: 324.14 (M + H).

5.1.26. N^1-([1,1′-biphenyl]-4-ylmethyl)-N^1-methyl-N^4-(5-methyl-1H-pyrazol-3-yl)maleamide (1f)

Using procedure D, starting from **6f** [17] (0.250 g, 1.27 mmol) and **12** (0.297 g, 1.52 mmol), 0.150 g of a white solid was obtained, with a purification with column chromatography (DCM/MeOH (NH_4OH 5 %) 9.5:0.5) (32 %). ^{1}H NMR (600Hz): δ 2.21 (s, 3H, CH_3-pyrazole), 2.81 (d, 3H, J = 19.4 Hz, NCH_3), 4.55 (d, 2H, J = 73.6, CH_2Ph), 6.27 (d, 1H, J = 11.9 Hz, C=CH), 6.37 (s, 1H, CH-pyrazole), 6.60 (dd, 1H, J = 30.4 and 11.9 Hz, C=CH), 7.33–7.41 (m, 2H, Ar), 7.43–7.51 (m, 3H, Ar), 7.59–7.69 (m, 4H, Ar), 10.64 (s, 1H, NH), 12.06 (NH-pyrazole). ^{13}C NMR: δ 10.67, (1C, CH_3-pyrazole), 31.44, 34.74 (1C, NCH_3), 48.55, 52.88 (1C, CH_2Ph), 95.70 (1C, CH-pyrazole), 126.63 (1C), 126.85 (2C), 127.33 (1C), 128.07 (1C), 128.40 (1C), 128.93 (2C), 135.28 (1C), 136.23 (1C), 136.63 (1C), 138.31 (1C), 138.92 (1C), 139.24 (1C), 139.80 (1C), 140.01 (1C), 147.16 (1C), 161.14 (1C, C=O), 167.92 (1C, C=O). MS (ES) *m/z*: 375.44 (M + H).

5.1.27. N^1-(4-(dimethylamino)benzyl)-N^1-methyl-N^4-(5-methyl-1H-pyrazol-3-yl)maleamide (1g)

Using procedure D, starting from **6g** [18] (0.560 g, 3.41 mmol) and **12** (0.734 g, 4.09 mmol), 0.300 g of a white solid was obtained, with a purification with column chromatography (DCM/MeOH (NH_4OH 5 %) 9.5:0.5) (26 %). ^{1}H NMR (600 MHz): δ 2.20 (s, 3H, CH_3-pyrazole), 2.71 (d, 3H, J = 11.6 Hz, NCH_3), 2.86 (d, 6H, J = 7.5 Hz, $N(CH_3)_2$), 4.36 (d, 2H, J = 78.9 Hz, CH_2Ph), 6.24 (dd, 1H, J = 17.2 and 11.9, C=CH), 6.35 (s, 1H, CH-pyrazole), 6.56 (dd, 1H, J = 52.3 and 11.9 Hz, C=CH), 6.64–6.71 (m, 2H, Ar), 7.09 (d, 1H, J = 8.6 Hz, Ar), 7.18 (d, 1H, J = 8.6 Hz, Ar), 10.61 (d, 1H, J = 8.8 Hz, NH), 12.05 (s, 1H, NH-pyrazole). ^{13}C NMR: δ 10.66 (1C, CH_3-pyrazole), 16.73 (1C, NCH_3), 18.09 (1C, NCH_3), 30.91, 34.18 (1C, $CONCH_3$), 48.14, 52.66 (1C, CH_2Ph), 95.70 (1C, CH-pyrazole), 112.35 (1C), 123.94 (1C), 124.53 (1C), 124.99 (1C), 125.58 (1C), 128.50 (1C), 128.90 (1C), 135.31 (1C), 138.27 (1C), 149.69 (1C), 161.10 (1C, C=O), 167.48 (1C, C=O). MS (ES) *m/z*: 342.42 (M + H).

5.1.28. N^1-(4-acetamidobenzyl)-N^1-methyl-N^4-(5-methyl-1H-pyrazol-3-yl)maleamide (1h)

Using procedure D, starting from **6h** [19] (0.118 g, 0.66 mmol) and **12** (0.154 g, 0.79 mmol), 0.075 g of a white solid was obtained, with a purification with column chromatography (DCM/MeOH (NH_4OH 5 %) 9.5:0.5) (32 %). ^{1}H NMR (600 MHz): δ 2.02 (d, 3H, J = 6.2 Hz, CH_3CO), 2.21 (d, 3H, J = 1.6 Hz, CH_3-pyrazole), 2.74 (d, 3H, J = 21.7 Hz, NCH_3), 4.43 (d, 2H, J = 81.1 Hz, CH_2Ph), 6.25 (dd, 1H, J = 11.9 and 2.3 Hz, C=CH), 6.33 (s, 1H, CH-pyrazole), 6.57 (dd, 1H, J = 34.2 and 11.9 Hz, C=CH), 7.20 (d, 1H, J = 8.5 Hz, Ar), 7.30 (d, 1H, J = 8.5 Hz, Ar), 7.48–7.57 (m, 2H, Ar), 9.91 (s, 1H, NH=$COCH_3$), 10.63 (s, 1H, NH), 10.06 (s, 1H, NH-pyrazole). ^{13}C NMR: δ 10.73 (1C, CH_3-pyrazole), 23.96 ($CO\underline{CH_3}$), 31.13, 34.50 (1C, NCH_3), 48.32, 52.76 (1C, CH_2PH), 95.58 (1C, CH-pyrazole), 118.93 (1C), 125.01 (1C), 125.63 (1C), 127.97 (1C), 128.16 (1C), 131.30 (1C), 131.73 (1C), 135.37 (1C), 138.24 (1C), 138.55 (1C), 161.12 (C=O), 167.68 (C=O), 168.17 (C=O). MS (ES) *m/z*: 356.40 (M + H).

5.1.29. N^1-methyl-N^4-(5-methyl-1H-pyrazol-3-yl)-N^1-(4-methylbenzyl) maleamide (1i)

Using procedure D, starting from **6i** [15] (0.410 g, 3.04 mmol) and **12** (0.711 g, 3.65 mmol), 0.200 g of a white solid was obtained, with a purification with column chromatography (DCM/MeOH (NH_4OH 5 %) 9.5:0.5) (21 %). ^{1}H NMR (600 MHz): δ 2.21 (s, 3H, CH_3-pyrazole), 2.28 (d, 3H, J = 11.0 Hz, CH_3), 2.74 (d, 3H, J = 18.4 Hz, NCH_3), 4.45 (d, 2H,

J = 78.3 Hz, CH_2Ph), 6.25 (d, 1H, J = 11.9 Hz, C=CH), 6.34 (s, 1H, CH-pyrazole), 6.57 (dd, 1H, J = 30.1 and 11.9 Hz, C=CH), 7.11–7.18 (m, 3H, Ar), 7.27 (d, 1H, J = 7.9 Hz, Ar), 10.62 (s, 1H, NH), 12.05 (s, 1H, NH-pyrazole). ^{13}C NMR: δ 10.70, (1C, CH_3-pyrazole), 20.71 (CH_3Ph), 31.21, 34.50 (1C, NCH_3), 48.48, 52.91 (1C, CH_2Ph), 95.68 (1C, CH-pyrazole), 125.04 (1C), 127.49 (1C), 127.79 (1C), 128.91 (1C), 129.11 (1C), 133.88 (1C), 134.23 (1C), 135.34 (1C), 136.03 (1C), 136.49 (1C), 161.12 (C=O), 167.78 (C=O). MS (ES) *m/z*: 313.74 (M + H).

5.1.30. N^1-(4-fluorobenzyl)-N^1-methyl-N^4-(5-methyl-1H-pyrazol-3-yl) maleamide (1j)

Using procedure D, starting from **6j** [20] (0.540 g, 3.88 mmol) and **12** (0.910 g, 4.66 mmol), 0.500 g of a white solid was obtained with an under vacuum filtration, without other purification (41 %). ^{1}H NMR (600 MHz): δ 2.21 (s, 3H, CH_3-pyrazole), 2.75 (d, 3H, J = 28.0 Hz, NCH_3), 4.48 (d, 2H, J = 75.0 Hz, CH_2Ph), 6.25 (dd, 1H, J = 11.9 Hz and 1.9 Hz, C=CH), 6.34 (s, 1H, CH-pyrazole), 6.58 (dd, 1H, J = 34.2 and 11.9 Hz, C=CH), 7.11–7.20 (m, 2H, Ar), 7.30–7.38 (m, 1H, Ar), 7.40–7.49 (m, 1H, Ar), 10.62 (d, 1H, J = 6.4 Hz, NH), 12.06 (s, 1H, NH-pyrazole). ^{13}C NMR: δ 10.70 (1C, CH_3-pyrazole), 31.22, 34.63 (1C, NCH_3), 48.13, 52.46 (1C, CH_2Ph), 95.73 (1C, CH-pyrazole), 114.99 (1C), 125.11 (1C), 125.77 (1C), 129.84 (1C), 133.16 (1C), 133.52 (1C), 135.34 (1C), 138.40 (1C), 160.59 (1C), 161.16 (1C), 162.19 (1C), 167.98 (1C). MS (ES) *m/z*: 317.34 (M + H).

5.1.31. N^1-benzyl-N^4-(5-methyl-1H-pyrazol-3-yl)maleamide (1k)

Using procedure D, starting from commercial *N*-benzylmethylamine **6k** (0.19 mL, 1.71 mmol) and **12** (0.400 g, 2.05 mmol), 0.160 g of a white solid was obtained, with a purification with column chromatography (DCM/MeOH (NH_4OH 5 %) 9.5:0.5) (33 %). ^{1}H NMR (600 MHz): δ 2.20 (s, 3H, CH_3-pyrazole), 4.38 (d, 2H, J = 5.9 Hz, CH_2Ph), 6.29 (q, 2H, J = 12.9 Hz, $(C{=}CH)_2$), 6.33 (s, 1H, CH-pyrazole), 7.19–7.29 (m, 1H, Ar), 7.29–7.36 (m, 4H, Ar), 9.33 (d, 1H, J = 6.4 Hz, CONHCH$_2$), 11.71 (s, 1H, CONH-pyrazole), 12.06 (s, 1H, NH-pyrazole). ^{13}C NMR: δ 10.64 (1C, CH_3), 42.33 (1C, CH_2), 95.81 (1C, CH-pyrazole), 126.93 (1C), 127.41 (2C), 128.33 (2C), 131.82 (1C, COCHCH), 132.16 (1C, COCHCH), 138.28 (1C), 138.73 (1C), 146.92 (1C) 161.54 (1C, CONH$(CH_2)(CH_3)$), 165.06 (1C, CONH-pyrazole). MS (ES) *m/z*: 285.32 (M + H).

5.1.32. N^1-benzyl-N^1-methyl-N^4-(5-methyl-1H-pyrazol-3-yl)fumaramide (2a)

Using procedure D, starting from 3-amino-5-methylpyrazole (0.046 g, 0.48 mmol) and **10a** (0.125 g, 0.57 mmol), 0.100 g of a white solid was obtained with an under vacuum filtration, without other purification (70 %). ^{1}H NMR (600 MHz): δ 2.20 (d, 3H, J = 12.4 Hz, CH_3-pyrazole), 2.99 (d, 3H, J = 74.8 Hz, NCH_3), 4.66 (d, 2H, J = 70.6 Hz, CH_2Ph), 6.36 (d, 1H, J = 32.1 Hz, C=CH), 7.09 (d, 1H, J = 18.0 Hz, C=CH), 7.19 (d, 1H, J = 6.6 Hz, C=CH), 7.23–7.27 (m, 1H, Ar), 7.27–7.32 (m, 1H, Ar), 7.32–7.43 (m, 3H, Ar), 10.81 (d, 1H, J = 11.4 Hz, CONH-pyrazole), 12.11 (s, 1H, NH -pyrazole). ^{13}C NMR (DMSO-d_6): δ 10.68 (1C, CH_3), 34.03, 35.10 (1C, NCH_3), 50.37, 52.58 (1C, CH_2Ph), 95.89 (1C,CH-pyrazole), 126.47 (1C), 127.18 (1C), 127.60 (1C), 128.55 (1C), 128.83 (1C), 130.26 (1C), 134.53 (1C), 137.33 (1C), 138.38 (1C), 147.15 (1C), 161.16 (1C, C=O), 164.64 (1C, C=O). MS (ES) *m/z*: 299.35 (M + H).

5.1.33. N^1-(4-methoxybenzyl)-N^1-methyl-N^4-(5-methyl-1H-pyrazol-3-yl) fumaramide (2b)

Using procedure D, starting from 3-amino-5-methylpyrazole (0.061 g, 0.63 mmol) and **10b** (0.190 g, 0.76 mmol), 0.150 g of white solid was obtained, with a purification with column chromatography (DCM/MeOH (NH_4OH 5 %) 9.75:0.25) (72 %). ^{1}H NMR (600 MHz): δ 2.20 (d, 3H, J = 8.1 Hz, CH_3-pyrazole), 2.95 (d, 3H, J = 69.8 Hz, NCH_3), 3.73 (d, 3H, J = 1.1 Hz, OCH_3), 4.57 (d, 2H, J = 66.4 Hz, CH_2Ph), 6.36 (d, 1H, J = 21.8 Hz, C=CH), 6.90 (d, 1H, J = 8.6 Hz, Ar), 6.94 (d, 1H, J = 8.7 Hz, Ar), 7.07 (dd, 1H, J = 15.0 and 5.0 Hz, C=CH), 7.10–7.15 (m, 1H, Ar), 7.17–7.22 (m, 1H, Ar), 7.37 (dd, 1H, J = 15.0 and 1.9 Hz, Ar), 10.81 (s, 1H, NH), 12.10 (s, 1H, NH-pyrazole). ^{13}C NMR: δ 10.67 (1C, CH_3), 33.75, 34.75 (1C, NCH_3), 49.95, 51.99 (1C, CH_2Ph), 55.08 (1C, OCH_3), 95.85 (1C, CH-pyrazole), 113.92 (1C), 114.20 (1C), 127.85 (1C), 129.11 (1C), 129.12 (1C), 129.21 (1C), 130.11 (1C), 130.34 (1C), 134.55 (1C), 158.49 (1C), 161.15 (1C, C=O), 164.71 (1C, C=O).

MS (ES) *m/z*: 329.37 (M + H).

5.1.34. N^1-(4-chlorobenzyl)-N^1-methyl-N^4-(5-methyl-1H-pyrazol-3-yl) fumaramide (2c)

Using procedure D, starting from 3-amino-5-methylpyrazole (0.063 g, 0.66 mmol) and **10c** (0.200 g, 0.79 mmol), 0.060 g of white solid, with a purification with column chromatography (DCM/MeOH (NH_4OH 5 %) 9.75:0.25) (29 %). ^{1}H NMR (600 MHz): δ 2.21 (d, 3H, J = 10.9 Hz, CH_3-pyrazole), 2.99 (d, 3H, J = 83.8 Hz, NCH_3), 4.66 (d, 2H, J = 80.2 Hz, CH_2Ph), 6.37 (d, 1H, J = 29.5 Hz, C=CH), 7.09 (d, 1H, J = 15.0 Hz, C=CH), 7.23 (d, 1H, J = 8.4 Hz, Ar), 7.27–7.32 (m, 1H, Ar), 7.40 (d, 1H, J = 9.2 Hz, Ar) 7.42 (d, 1H, J = 2.4 Hz, Ar), 7.46 (d, 1H, J = 8.4 Hz, Ar), 10.82 (d, 1H, J = 12.2 Hz, NH), 12.12 (s, 1H, NH-pyrazole). ^{13}C NMR: δ 10.66 (1C, CH_3), 33.99, 35.13 (1C, NCH_3), 49.77, 51.91 (1C, CH_2Ph), 95.87 (1C, CH-pyrazole), 128.42 (1C), 128.48 (1C), 128.77 (1C), 129.51 (1C), 130.10 (1C), 131.75 (1C), 134.61 (1C), 136.42 (1C), 138.36 (1C), 147.12 (1C), 161.10 (1C, C=O), 164.68 (1C, C=O). MS (ES) *m/z*: 333.79 (M + H).

5.1.35. N^1-benzyl-N^1-methyl-N^4-(5-methyl-1H-pyrazol-3-yl)succinamide (3a)

Using procedure D, starting from 3-amino-5-methylpyrazole (0.107 g, 1.1 mmol) and **8a** (0.292 g, 1.3 mmol), 0.220 g of white solid was obtained, with a purification with column chromatography (DCM/MeOH (NH_4OH 5 %) 9.75:0.25) (67 %). ^{1}H NMR (600 MHz): δ 2.17 (d, 3H, J = 5.7 Hz, CH_3-pyrazole), 2.52–2.58 (m, 2H, CH_2CO), 2.59–2.68 (m, 2H, CH_2CO), 2.86 (d, 3H, J = 88.4 Hz, NCH_3), 4.55 (d, 2H, J = 60.3 Hz), 6.24 (d, 1H, J = 14.7 Hz, CH-pyrazole), 7.17–7.22 (m, 1H, Ar), 7.22–7.24 (m, 3H, Ar), 7.38 (t, 1H, J = 7.6 Hz, Ar), 10.18 (d, 1H, J = 11.2 Hz, NH), 11.89 (s, 1H, NH-pyrazole). ^{13}C NMR: 10.68 (1C, CH_3), 27.77 (1C, CH_2), 30.66 (1C, CH_2), 33.39, 34.62 (1C, NCH_3), 49.96, 52.23 (1C, CH_2Ph), 95.47 (1C, CH-pyrazole), 126.59 (1C), 126.91 (1C), 127.20 (1C), 127.38 (1C), 128.40 (1C), 137.47 (1C), 137.86 (1C), 169.51 (1C, C=O), 171.51 (1C, C=O). MS (ES) *m/z*: 301.36 (M + H).

5.1.36. N^1-(4-methoxybenzyl)-N^1-methyl-N^4-(5-methyl-1H-pyrazol-3-yl) succinamide (3b)

Using procedure D, starting from 3-amino-5-methylpyrazole (0.080 g, 0.83 mmol) and **8b** (0.234 g, 1.0 mmol), 0.190 g of white solid was obtained, with a purification with column chromatography (DCM/MeOH 9.5:0.5) (69 %). ^{1}H NMR (600 MHz): δ 2.18 (s, 3H, CH_3-pyrazole), 2.51–2.56 (m, 2H, CH_2), 2.58–2.66 (m, 2H, CH_2), 2.82 (d, 3H, J = 84.9 Hz, NCH_3), 3.73 (d, 3H, J = 13.0 Hz, OCH_3), 4.46 (d, 2H, J = 56.3 Hz, CH_2Ph), 6.23 (d, 1H, J = 10.1 Hz, CH-pyrazole), 6.90 (dd, 2H, J = 43.1 and 8.6 Hz, Ar), 7.15 (dd, 2H, J = 26.7 and 8.6 Hz, Ar), 10.17 (d, 1H, J = 8.2 Hz, NH), 11.89 (s, 1H, NH-pyrazole). ^{13}C NMR: δ 10.70 (1C, CH_3), 27.86 (1C, CH_2), 30.71 (1C, CH_2), 33.17, 34.36 (1C, NCH_3), 49.31, 51.68 (1C, CH_2Ph), 55.05 (1C, OCH_3), 95.52 (1C, CH-pyrazole), 113.84 (1C), 128.04 (1C), 128.89 (1C), 129.23 (1C), 129.78 (1C), 138.00 (1C), 147.63 (1C), 158.34 (1C), 169.57 (1C), 171.39 (1C). MS (ES) *m/z*: 331.39 (M + H).

5.1.37. N^1-(4-chlorobenzyl)-N^1-methyl-N^4-(5-methyl-1H-pyrazol-3-yl) succinamide (3c)

Using procedure D, starting from 3-amino-5-methylpyrazole (0.055

g, 0.56 mmol) and **8c** (0.174 g, 0.68 mmol), 0.140 g of white solid was obtained, with a purification with column chromatography (DCM/MeOH (NH_4OH 5 %) 9.75:0.25) (75 %). ^{1}H NMR (600 MHz): δ 2.17 (d, 3H, J = 5.5 Hz, CH_3-pyrazole), 2.51–2.57 (m, 2H, CH_2), 2.62 (dt, 2H, J = 25.9, 6.7 Hz, CH_2), 2.86 (d, 3H, J = 96.1 Hz, NCH_3), 4.54 (d, 2H, J = 68.4 Hz, CH_2Ph), 6.23 (d, 1H, J = 12.4 Hz, CH-pyrazole), 7.25 (dd, 2H, J = 29.5 and 8.4 Hz, Ar), 7.40 (dd, 2H, J = 48.0 and 8.4 Hz, Ar), 10.18 (d, 1H, J = 10.9 Hz, NH), 11.90 (s, 1H, NH-pyrazole). ^{13}C NMR: δ 10.68 (1C, CH_3-pyrazole), 27.74 (1C, CH_2), 30.65 (1C, CH_2), 33.37, 34.69 (1C, NCH_3), 49.39, 51.60 (1C, CH_2Ph), 95.49 (1C, CH-pyrazole), 128.35 (1C), 128.57 (1C), 129.30 (1C), 131.49 (1C), 131.76 (1C), 136.60 (1C), 136.69 (1C), 137.96 (1C), 169.49 (1C, C=O), 171.66 (1C, C=O). MS (ES) *m/z*: 334.80 (M + H).

5.1.38. N^1-benzyl-N^1-methyl-N^5-(5-methyl-1H-pyrazol-3-yl)glutaramide (4a)

Using procedure D, starting from 3-amino-5-methylpyrazole (0.043 g, 0.44 mmol) and **9a** (0.125 g, 0.53 mmol), 0.100 g of white solid was obtained, with a purification with column chromatography (DCM/MeOH (NH_4OH 5 %) 9.5:0.5) (72 %). ^{1}H NMR (600 MHz): δ 1.74–1.85 (m, 2H, $CH_2\underline{CH_2}CH_2$), 2.17 (d, 3H, J = 4.4 Hz, CH_3-pyrazole), 2.30 (dt, 2H, J = 30.0 and 7.3 Hz, $N(CH_3)(CH_2)CO\underline{CH_2}$), 2.37 (dt, 2H, J = 17.7 and 7.4 Hz, $NHCO\underline{CH_2}$), 2.84 (d, 3H, J = 56.7 Hz, NCH_3), 4.53 (d, 2H, J = 30.3 Hz, CH_2Ph), 6.23 (d, 1H, J = 22.1 Hz, CH-pyrazole), 7.15–7.22 (m, 2H, Ar), 7.22–7.30 (m, 1H, Ar), 7.30–7.38 (m, 2H, Ar), 10.14 (d, 1H, J = 23.9 Hz, NH), 11.90 (s, 1H, NH-pyrazole). ^{13}C NMR: δ 10.69 (1C, CH_3), 20.69 (1C; CH_2), 31.59 (1C, CH_2), 31.90 (1C, CH_2), 33.33, 34.64 (1C, NCH_3), 49.83, 52.30 (1C, CH_2Ph), 95.54 (1C, CH-pyrazole), 126.49 (1C), 126.92 (1C), 127.17 (1C), 127.40 (1C), 128.44 (1C), 128.71 (1C), 137.50 (1C), 137.94 (1C), 169.91 (1C, C=O), 171.88 (1C, C=O). MS (ES) *m/z*: 315.39 (M + H).

5.1.39. N^1-(4-methoxybenzyl)-N^1-methyl-N^5-(5-methyl-1H-pyrazol-3-yl) glutaramide (4b)

Using procedure D, starting from 3-amino-5-methylpyrazole (0.080 g, 0.83 mmol) and **9b** (0.231 g, 0.99 mmol), 0.150 g of white solid was obtained, with a purification with column chromatography (DCM/MeOH 9.5:0.5) (53 %). ^{1}H NMR (600 MHz): δ 1.72–1.85 (m, 2H, $CH_2\underline{CH_2}CH_2$), 2.17 (d, 3H, J = 2.5 Hz, CH_3-pyrazole), 2.30 (dt, 2H, J = 18.6 and 7.3 Hz, CH_2), 2.36 (dt, 2H, J = 10.4 and 7.4 Hz, CH_2), 2.80 (d, 3H, J = 51.9 Hz, NCH_3), 3.72 (d, 3H, J = 2.8 Hz, OCH_3), 4.44 (d, 2H, J = 23.6 Hz, CH_2Ph), 6.24 (d, 1H, J = 13.6 Hz, CH-pyrazole), 6.84–6.91 (m, 2H, Ar), 7.12 (dd, 2H, J = 20.6 and 8.6 Hz, Ar), 10.14 (d, 1H, J = 11.8 Hz, NH), 11.91 (s, 1H, NH-pyrazole). ^{13}C NMR: δ 10.70 (1C, CH_3), 20.71 (1C, CH_2), 31.58, 31.96 (1C, CH_2), 33.09 (1C, CH_2), 34.36, 34.79 (1C, NCH_3), 49.15, 51.72 (1C, CH_2Ph), 55.03 (1C, OCH_3), 95.56 (1C, CH-pyrazole), 113.86 (1C), 114.10 (1C), 127.91 (1C), 128.90 (2C), 129.22 (1C), 129.85 (1C), 158.34 (1C), 169.94 (1C, C=O), 171.74 (1C, C=O). MS (ES) *m/z*: 345.42 (M + H).

5.1.40. N^1-(4-chlorobenzyl)-N^1-methyl-N^5-(5-methyl-1H-pyrazol-3-yl) glutaramide (4c)

Using procedure D, starting from 3-amino-5-methylpyrazole (0.089 g, 0.92 mmol) and **9c** (0. 275 g, 1.1 mmol), 0.270 g of white solid was obtained, with a purification with column chromatography (DCM/MeOH (NH_4OH 5 %) 9.75:0.25) (78 %). ^{1}H NMR (600 MHz): δ 1.74–1.84 (m, 2H, $CH_2\underline{CH_2}CH_2$), 2.17 (s, 3H, CH_3-pyrazole), 2.24–2.41 (m, 4H, CH_2), 2.84 (d, 3H, J = 61.3 Hz, NCH_3), 4.51 (d, 2H, J = 35.9 Hz, CH_2Ph), 6.23 (d, 1H, J = 26.3 Hz, CH-pyrazole), 7.21 (dd, 2H, J = 20.5 and 8.4 Hz, Ar), 7.38 (dd, 2H, J = 8.4 and 1.9 Hz, Ar), 10.13 (d, 1H, J = 20.9 Hz, NH), 11.91 (s, 1H, NH-pyrazole). ^{13}C NMR: δ 10.66 (1C, CH_3), 20.65 (1C, CH_2), 31.50 (1C, CH_2), 31.86 (1C, CH_2), 33.34, 34.70 (1C, NCH_3), 49.27, 51.65 (1C, CH_2Ph), 95.59 (1C, CH-pyrazole), 128.40 (1C), 128.67 (1C), 129.35 (1C), 131.52 (1C), 131.73 (1C), 136.59 (1C), 137.06 (1C), 138.01 (1C), 169.91 (1C, C=O), 172.02 (1C, C=O). MS (ES) *m/z*: 349.83 (M + H).

5.1.41. N^1-benzyl-N^1-methyl-N^2-(5-methyl-1H-pyrazol-3-yl)oxalamide (5a)

Using procedure D, starting from 3-amino-5-methylpyrazole (0.080 g, 0.83 mmol) and **11a** (0.379 g, 1.0 mmol), 0.180 g of white solid was obtained, with a purification with column chromatography (DCM/MeOH (NH_4OH 5 %) 9.75:0.25) (78 %). ^{1}H NMR (600 MHz): δ 2.20 (d, 3H, J = 12.4 Hz, CH_3-pyrazole), 2.80 (d, 3H, J = 80 Hz, NCH_3), 4.53 (d, 2H, J = 20.5 Hz, CH_2Ph), 6.28 (d, 1H, J = 11.4 Hz, CH-pyrazole), 7.28–7.34 (m, 2H, Ar), 7.35–7.39 (m, 3H, Ar), 11.04 (d, 1H, J = 6.7 Hz, NH), 12.15 (d, 1H, J = 8.1 Hz, NH-pyrazole). ^{13}C NMR: δ 10.43 (1C, CH_3), 30.91, 34.38 (1C, NCH_3), 48.56, 52.47 (1C, CH_2Ph), 95.89 (1C, CH-pyrazole), 127.17 (1C), 127.50 (1C), 127.65 (1C), 128.35 (1C), 136.20 (1C), 138.41 (1C), 145.62 (1C), 145.70 (1C), 161.39 (1C, C=O), 164.27 (1C, C=O). MS (ES) *m/z*: 273.31 (M + H).

5.1.42. N^1-(4-methoxybenzyl)-N^1-methyl-N^2-(5-methyl-1H-pyrazol-3-yl) oxalamide (5b)

Using procedure D, starting from 3-amino-5-methylpyrazole (0.045 g, 0.47 mmol) and **11b** (0.213 g, 0.56 mmol), 0.080 g of white solid was obtained, with a purification with column chromatography (DCM/MeOH (NH_4OH 5 %) 9.9:0.1) (56 %). ^{1}H NMR (600 MHz): δ 2.20 (d, 3H, J = 6.6 Hz, CH_3-pyrazole), 2.77 (d, 3H, J = 77.1 Hz, NCH_3), 3.75 (d, 3H, J = 3.4 Hz, OCH_3), 4.44 (d, 2H, J = 28.6 Hz, CH_2Ph), 6.28 (s, 1H, CH-pyrazole), 6.92 (d, 2H, J = 8.6 Hz, Ar), 7.28 (dd, 2H, J = 30.0 Hz and 8.6 Hz, Ar), 11.02 (d, 1H, J = 10.7 Hz, NH), 12.14 (s, 1H, NH-pyrazole). ^{13}C NMR: δ 10.61 (1C, CH_3-pyrazole), 30.74, 34.28 (1C, NCH_3), 48.10, 52.05 (1C, CH_2Ph), 55.08 (1C, OCH_3), 96.08 (1C, CH-pyrazole), 113.92 (1C), 127.88 (1C), 128.24 (1C), 129.27 (1C), 129.36 (1C), 138.58 (1C), 145.81 (1C), 158.84 (1C), 161.71 (1C, C=O), 164.28 (1C, C=O). MS (ES) *m/z*: 303.33 (M + H).

5.1.43. N^1-(4-chlorobenzyl)-N^1-methyl-N^2-(5-methyl-1H-pyrazol-3-yl) oxalamide (5c)

Using procedure D, starting from 3-amino-5-methylpyrazole (0.053 g, 0.55 mmol) and **11c** (0.150 g, 0.66 mmol), 0130 g of white solid was obtained, with a purification with column chromatography (DCM/MeOH (NH_4OH 5 %) 9.5:0.5) (77 %). ^{1}H NMR (600 MHz): δ 2.20 (d, 3H, J = 12.1 Hz, CH_3-pyrazole), 2.80 (d, 3H, J = 80.5 Hz, NCH_3), 4.52 (d, 2H, J = 20.3 Hz, CH_2Ph), 6.28 (d, 1H, J = 15.1 Hz, CH-pyrazole), 7.33–7.42 (m, 2H, Ar), 7.42–7.46 (m, 2H, Ar), 11.04 (d, 1H, J = 15.2 Hz, NH), 12.15 (d, 1H, J = 9.5 Hz, NH-pyrazole). ^{13}C NMR: δ 10.58 (1C, CH_3-pyrazole), 31.12, 34.59 (1C, NCH_3), 48.12, 51.97 (1C, CH_2Ph), 96.03 (1C, CH-pyrazole), 128.47 (1C), 129.76 (1C), 131.97 (1C), 132.30 (1C), 135.26 (1C), 135.48 (1C), 138.60 (1C), 145.85 (1C), 161.48 (1C, C=O), 164.51 (1C, C=O). MS (ES) *m/z*: 307.75 (M + H).

5.2. Determination of GSK-3β inhibitory activity by LANCE ultra TR-FRET

LANCE Ultra TR-FRET assays were performed at room temperature (22 °C). Enzymatic reactions were conducted in white Optiplate-384 in a final volume of 25 μL, diluting all the reagents in kinase buffer (50 mM HEPES pH 7.5, 1 mM EGTA, 10 mM $MgCl_2$, 2 mM DTT, and 0.01 % Tween-20). The compounds, dissolved in DMSO, were diluted in kinase buffer, keeping constant the percentage of DMSO (2 %) in each well. The compound SB216763 was used as a positive control (IC_{50} 11.4 ± 2.1 nM), while DMSO was used as reference (100 % enzymatic activity).

The enzyme GSK-3β (0.5 nM, final concentration) was initially incubated with the compounds for 30 min, then a mixture of co-factor ATP (10 μM, final concentration) and substrate ULight-GS(Ser641/pSer657) peptide (50 nM, final concentration) was added in subdued light. The reaction was incubated in the dark for 1 h at room temperature. Afterwards, the addition of 24 mM EDTA and 2 nM (final concentration) of Eu-antiphospho-GS (Ser641) antibody, both diluted in detection buffer, stopped the enzymatic reaction. After a second incubation of 1 h, the TR-FRET signal was read with the Ensight multimode

plate reader (excitation at 320 nm and emissions at 615 and 665 nm). Data were analyzed using Excel and GraphPad Prism software (version 9.0). Values obtained for each compound are the means ± SD determined for at least two separate experiments. For the determination of IC_{50}, the compounds were tested in 10 doses with 2-fold serial dilutions and the data were fitted using "log(inhibitor) *vs*. response - variable slope (four parameters)" equation.

5.3. Testing for reversibility of 1c by MMSA

The **1c** reversible mechanism of inhibition was investigated by MMSA, monitoring in real-time the GSK-3β enzymatic activity. **1c** compound was incubated at 10x its IC_{50} value (15.6 μM) with 100x GSK-3β (100 nM) for 30 min at room temperature (22 °C). Then, the mixture was diluted 100x with the reaction buffer (50 mM Hepes pH 7.4, 1 mM EGTA, 10 mM $MgCl_2$, 2 mM DTT, 0.01 % w/v Tween-20) containing 1x fluorescein-labeled peptide substrate (5-FAM-KRREILSRRPpSYR-COOH, ProfilerPro Peptide 15, # 760359, PerkinElmer) and 10 μM ATP. In parallel, blank (without **1c** inhibitor and enzyme) and untreated samples (with enzyme and without **1c** inhibitor) were prepared in the same reaction buffer. 25 μL of each sample was transferred to a black low-volume 384-well microplate, and the enzymatic reaction was monitored in real-time (kinetic mode) every 2 min for 100 min on Caliper Life Sciences EZ reader II. The separation conditions employed to detect fluorescein substrate and product of enzymatic reaction were −1.2 psi pressure, −2500 V upstream voltage, −500 V downstream voltage, 35 s post-sample buffer sip time, and 110 s final delay. The amount of product formed was determined as a percentage of conversion by calculating the ratio of the product peak heights/(product + substrate peak heights).

5.4. Testing for reversibility of 1c by Jump-Dilution test

The reversibility inhibition profile of **1c** was determined by the application of a jump dilution experiment performed by LANCE Ultra TR-FRET assay. Before proceeding with the enzymatic reaction, 5 μL of a 100x solution containing GSK-3β (50 nM) was pre-incubated with 2.5 μL of a 10x the biochemical IC_{50} of **1c** for 30 min. Subsequently, this solution was diluted 100-fold into the buffer containing substrate and co-factor, allowing the beginning of the phosphorylation reaction. This dilution creates a 1x solution of the protein while it dilutes the compound from 10x to 0.1x the IC_{50} value. The residual enzymatic activity was measured, and values are reported as percentage activity (mean values ± SD of two separate experiments) compared to the reaction performed with the vehicle (DMSO).

5.5. Mechanism of action studies by MMSA

The mechanism of action of **1c** was investigated by a preliminary experiment at four different ATP concentrations (36, 18, 9, and 4.5 μM), keeping constant **1c** concentration at its IC_{50} value (1.56 μM), and by a double titration experiment with six concentrations of **1c** (3.13, 1.56, 0.78, 0.39, 0.20, and 0.10 μM) and five ATP concentrations (36, 18, 9, 4.50, and 2.25 μM). For both experiments, each well of a black low-volume 384-well microplate was filled with 6.25 μL of 2 μM peptide substrate (4x), 6.25 μL of **1c** (4x), 6.25 μL of ATP (4x), and 6.25 μL of 4 nM GSK-3β (4x). Positive and negative control samples were also prepared by substituting the inhibitor with the reaction buffer supplemented with 4 % DMSO (4x), and for negative control, ATP was substituted with the reaction buffer (50 mM Hepes pH 7.4, 1 mM EGTA, 10 mM $MgCl_2$, 2 mM DTT, 0.01 % w/v Tween-20). The enzymatic reaction was monitored in real-time (kinetic mode), every 2 min for 70 min, on Caliper Life Sciences EZ reader II, and the separation conditions employed to detect fluorescein substrate and product were −1.2 psi pressure, −2500 V upstream voltage, −500 V downstream voltage, 35 s post-sample buffer sip time, and 110 s final delay. The amount of product formed was determined as a percentage of conversion by calculating the ratio of the product peak heights/(product + substrate peak heights). The percentages of conversion over time for each ATP concentration were analyzed through linear regression, and the slopes obtained were plotted to the co-factor concentration using the Michaelis-Menten equation to obtain K_M and V_{max} values.

5.6. Inhibition of $A\beta_{42}$ self-aggregation

The inhibitory potency was evaluated by screening the selected compounds at 1:1 ratio with $A\beta_{42}$. To assess $A\beta_{42}$ aggregation (and inhibition) the Thioflavin T fluorescence method was applied [43,60]. Briefly, 1,1,1,3,3,3-hexafluoro-2-propanol (HFIP) pretreated $A\beta_{42}$ samples (Bachem AG, Switzerland) were solubilized using a mixture of CH_3CN, 0.3 mM Na_2CO_3, and 250 mM NaOH (48.4/48.4/3.2) to obtain a stable stock solution with a concentration of 500 μM. For inhibition experiments, the peptide at a final concentration of 50 μM was incubated with and without inhibitor (50 μM, $A\beta_{42}$/inhib. = 1/1) in 10 mM phosphate buffer pH 8.0 containing 10 mM NaCl, at 30 °C for 24 h. After incubation, the samples were diluted to a final volume of 2.0 mL with 50 mM glycine-NaOH buffer (pH 8.5) containing 1.5 μM Thioflavin T to account for amyloid fibril formation. Then, a 300-s time scan of fluorescence intensity was carried out at λem = 490 nm (setting λexc at 446 nm), and values at the plateau were averaged after subtracting the background fluorescence of the Thioflavin T solution. Fluorescence intensities recorded in the absence and presence of inhibitor were compared, and the percentage inhibition due to the presence of the tested inhibitor was calculated.

5.7. Chelation studies by differential spectroscopy

UV–vis absorption spectra were recorded at room temperature by using a Jasco V530 double-beam spectrometer (Jasco Europe, Italy). Stock solutions of compounds **1b**, **1c**, **3c**, and **4c** (2 mM) were prepared in methanol, while solutions of $CuCl_2$ (10 mM) and $ZnCl_2$ (10 mM) were prepared either in methanol or bidistilled water. For chelation experiments, a fixed concentration of the compound under evaluation (40 μM) was added to growing concentrations of metal (either copper or zinc) ranging from 5 to 80 μM (final concentration). UV–vis spectra (205–400 nm) were recorded vs pure solvent. Spectra of the tested compound alone (at 40 μM) and metal ion alone at increasing concentrations (from 5 to 80 μM) were also recorded in the same experimental conditions. Studies were conducted in both methanol and water. To obtain the differential spectra, the spectra of either **3c** or **4c** and that of the metal alone (at the corresponding molar concentration) were mathematically subtracted from the spectrum of the Cu(II):L complex.

5.8. MTT on SH-SY5Y

Neuroblastoma cell line SH-5H5Y was cultured in DMEM supplemented with 10 % (v/v) fetal bovine serum, 100 U/mL penicillin, 100 μg/mL streptomycin, and 2 mM L-glutamine, at 37 °C in a 5 % CO_2 atmosphere.

The cytotoxicity of compounds was determined via a 3-(4,5-dimethylthiazol-2-yl)-2,5-diphenyltetrazoliumbromide (MTT) assay. A total of 200 μL of cells (3×10^4 cells/mL) was seeded in a 96-well microtiter plate and was subsequently exposed to three different concentrations of compounds (50, 10 and 2 μM) for 24 h, keeping constant the concentration of DMSO (1 %). The mitochondrial-dependent reduction of MTT to formazan was used to assess cell viability. Live cells reduce yellow MTT to purple formazan. The resulting formazan crystals were solubilized in DMSO, and the absorbance was measured at 550 nm and corrected for the background at 620 nm. Experiments were performed in quadruplicate and all values are expressed as the percentage of viability with respect to the control (1 % DMSO).

5.9. MTT on cerebellar granule neurons (CGNs)

Primary cerebellar granule cells were dissociated from cerebella and plated on 96-well plates, previously coated with 10 μg/mL poly-L-lysine, at a density of 1.2×10^5 cells/0.2 mL medium/well in BME supplemented with 10 % heat-inactivated FBS (Life Technologies), 2 mmol/L glutamine, 100 μmol/L gentamicin sulfate and 25 mM KCl (all from Sigma-Aldrich). Sixteen hours later, 10 μM cytosine arabinofuranoside (Sigma-Aldrich) was added to avoid glial proliferation. After 7 days *in vitro*, differentiated neurons were shifted to serum free BME medium and exposed to increasing concentration (5 μM, 10 μM, 25 μM) of compounds of interest (**1c** and **4c**) for 24 h. Then, cell viability was evaluated through the MTT assay.

5.10. Neuroprotective effect in CGNs

To evaluate the neuroprotective effect of our compounds, we tested increasing concentration (5 μM, 10 μM, 25 μM) of compounds of interest (**1c** and **4c**) on differentiated CGNs switched to serum-free BME medium with 5 mM KCl (serum-potassium deprivation) for 48 h to mimic *in vitro* the naturally occurring death of granule cells. Neuroprotection was evaluated through MTT assay.

5.11. Immunomodulation in N9 cell line

N9 microglial cells were plated at a density of 1.2 x 105 cell/35 mm Ø dish in serum free DMEM High Glucose (Life Technologies) and pretreated (2 h) with increasing concentrations of compounds (**1c** and **4c**) (2.5 μM, 5 μM) in the presence of LPS (Lipopolysaccharides from *Escherichia coli* O26:B6; CAS No.: 93572-42-0, Sigma-Aldrich, St. Louis, MO, United States) 100 ng/ml for 24 h. The microglial phenotype was evaluated through Western blot analysis of the pro-inflammatory-iNOS (inducible Nitric Oxide Synthase) and anti-inflammatory-TREM2 (Triggering Receptor Expressed on Myeloid cells 2) markers. Briefly, 24 h after treatments, microglial cells were lysed in ice-cold lysis buffer (50 mM Tris-HCl pH 7.4, 1 % SDS, 0.05 % protease inhibitor cocktail, Sigma-Aldrich, St. Louis, MO, United States), sonicated and protein concentration determined by using the Lowry method (Lowry, O. H. et al., 1951). 20 μg of protein were resuspended in 4X LB, tempered at 95 °C, subjected to thermal shock and loaded onto 10 % sodium dodecyl sulfate-polyacrylamide gels (SDS-PAGE; Bio-Rad Laboratories S.r.l., Segrate, MI, Italy). Electrophoresis was followed by transfer onto nitrocellulose membranes (GE Healthcare Europe GmbH, Milano, MI, IT) and blocking for 1 h in 5 % nonfat milk (Bio-Rad Laboratories S.r.l., Segrate, MI, Italy) in 0.1 % Tween-20 in PBS. Membranes were then incubated overnight at 4 °C with the following primary antibodies; anti-iNOS, (1:1000 dilution in PBS-0.1 % Tween-20, Cell Signaling Technology Inc., Massachusetts, USA), anti-TREM2 (1:1000 dilution in PBS-0.1 % Tween-20, Thermo-Fisher, Waltham, Massachusetts, United States), and anti-GAPDH (1:20000 dilution in PBS-0.1 % Tween-20, Santa Cruz Biotechnology Dallas, Texas, United States). Membranes were then incubated with HRP-conjugated secondary antibody Goat anti-Mouse or Goat anti-Rabbit (1:5000 dilution in PBS-0.1 % Tween-20, Jackson ImmunoResearch, West Grove, Pennsylvania, United States) for 90 min at RT. Labeled proteins were visualized by using the Clarity™ Western ECL Substrate and images acquired by using the ChemiDoc™ MP imaging system (Bio-Rad Laboratories S.r.l., Segrate, MI, Italy). Densitometric analysis was performed by using Bio-Rad Image Lab software 6.0.0.

5.11.1. Statistical analysis

Data were analyzed by using the GraphPad Prism8, San Diego, CA, United States software and expressed as a mean ± standard error of independent experiments. One-way ANOVA followed by Dunnett's post-hoc was used to compare the means between control and treated cells. Only p-values <0.05 were considered statistically significant.

5.12. PAMPA-BBB

0.50 mM donor solutions for furosemide, caffeine, and propranolol, 0.10 mM donor solution for piroxicam, and 0.25 mM donor solution for compound **1c** were prepared by diluting 50 mM dimethyl sulfoxide (DMSO) stock solutions with 1x phosphate buffer saline (PBS) pH 7.4, keeping the final DMSO concentration at 20 %.

The artificial lipid membrane solution was prepared by dissolving in dodecane the porcine brain polar lipid extract powder at 2 % (w/v) (BBB-specific lipid solution, Avanti Polar Lipids, #141101). The 96-well microfilter plates (MultiScreen®-IP, 0.45 μm, catalogue no. MAIPN4550) and the 96-well microtiter plate (MultiScreen®-acceptor, catalogue no. MSSACCEPTOR) were used as donor and acceptor compartments. Filters of donor plates were coated with 5 μL of freshly prepared artificial membrane solution.

After applying the lipids, acceptor plate wells were charged with 300 μL of 1x PBS, pH 7.4–20 % DMSO solution. Donor filter plates, charged with 150 μL of donor solutions, were placed onto the acceptor plates. The resulting sandwich was incubated for 24 h at room temperature, under stirring on Heidolph TITRAMAX 100 (600 rpm). Then, the sandwich plates were separated, and concentrations were determined. Acceptor solutions were transferred to a UV quartz microtiter plate and measured by UV spectroscopy, using Multiskan GO microplate spectrophotometer (Thermo Fisher Scientific) in spectrum mode (200–800 nm) at a step of 5 nm. Equilibrium solutions were prepared in parallel by diluting the donor solutions (150 μL) to 450 μL, and concentration was also measured by UV spectroscopy.

All compounds were assayed in duplicate, and the apparent (P_{app}, $LogP_{app}$) values were reported as mean ± standard deviation. The apparent permeability value, P_{app}, was calculated based on the Faller modification of the Sugano equation:

$$P_{app} = - [(V_D V_R) / (V_D + V_R) * At] * \ln (1 - r)$$

V_R is the volume of the acceptor compartment (0.300 cm^3), V_D is the donor volume (0.150 cm^3), A is the accessible filter area (0.266 cm^2), t is the incubation time in seconds, and r is the ratio of acceptor and equilibrium solution concentrations.

CRediT authorship contribution statement

Rebecca Orioli: Writing – original draft, Validation, Methodology, Data curation. **Giuliana Sarno:** Validation, Investigation, Data curation. **Francesca Seghetti:** Visualization, Methodology, Data curation. **Silvia Gobbi:** Writing – review & editing, Validation, Formal analysis. **Federica Belluti:** Writing – review & editing, Validation, Formal analysis. **Alessandra Feoli:** Writing – review & editing, Methodology, Investigation, Data curation. **Francesca Massenzio:** Validation, Methodology, Investigation, Data curation. **Barbara Monti:** Validation, Supervision, Data curation. **Rosaria Spagnuolo:** Methodology, Investigation. **Manuela Bartolini:** Writing – review & editing, Validation, Supervision, Data curation. **Sabrina Castellano:** Writing – review & editing, Writing – original draft, Supervision, Conceptualization. **Alessandra Bisi:** Writing – review & editing, Writing – original draft, Supervision, Project administration, Conceptualization.

Declaration of competing interest

The authors declare that they have no known competing financial interests or personal relationships that could have appeared to influence the work reported in this paper.

Appendix A. Supplementary data

Supplementary data to this article can be found online at https://doi.org/10.1016/j.ejmech.2025.117799.

Data availability

The datasets generated and/or analyzed during the current study are available in the AMS Acta repository

References

[1] H.-J. Cho, A.K. Sharma, Y. Zhang, M.L. Gross, L.M. Mirica, A multifunctional chemical agent as an attenuator of amyloid burden and neuroinflammation in alzheimer's disease, ACS Chem. Neurosci. 11 (2020) 1471–1481, https://doi.org/10.1021/acschemneuro.0c00114.

[2] A.A. Turab Naqvi, G.M. Hasan, MdI. Hassan, Targeting tau hyperphosphorylation via kinase inhibition: strategy to address alzheimer's disease, Curr. Top. Med. Chem. 20 (2020) 1059–1073, https://doi.org/10.2174/1568026620666200106125910.

[3] V. Calsolaro, P. Edison, Neuroinflammation in Alzheimer's disease: current evidence and future directions, Alzheimer's & Dementia 12 (2016) 719–732, https://doi.org/10.1016/j.jalz.2016.02.010.

[4] 2025 Alzheimer's disease facts and figures, Alzheimer's & Dementia 21 (2025), https://doi.org/10.1002/alz.70235.

[5] N. Chauhan, S. Paliwal, S. Jain, K. Verma, S. Paliwal, S. Sharma, GSK-3β and its inhibitors in alzheimer's disease: a recent update, Mini Rev. Med. Chem. 22 (2022) 2881–2895, https://doi.org/10.2174/1389557522666220420094317.

[6] S. Demuro, R.M.C. Di Martino, J.A. Ortega, A. Cavalli, GSK-3β, FYN, and DYRK1A: master regulators in neurodegenerative pathways, Int. J. Mol. Sci. 22 (2021) 9098, https://doi.org/10.3390/ijms22169098.

[7] L. Xing, J. Klug-Mcleod, B. Rai, E.A. Lunney, Kinase Hinge binding scaffolds and their hydrogen bond patterns, Bioorg. Med. Chem. 23 (2015) 6520–6527, https://doi.org/10.1016/j.bmc.2015.08.006.

[8] G.M. Nitulescu, G. Stancov, O.C. Seremet, G. Nitulescu, D.P. Mihai, C.G. Duta-Bratu, S.F. Barbuceanu, O.T. Olaru, The importance of the pyrazole scaffold in the design of protein kinases inhibitors as targeted anticancer therapies, Molecules 28 (2023) 5359, https://doi.org/10.3390/molecules28145359.

[9] C.N. Kirsten, T.H. Schrader, Intermolecular β-Sheet stabilization with aminopyrazoles, J. Am. Chem. Soc. 119 (1997) 12061–12068, https://doi.org/10.1021/ja972158y.

[10] P. Rzepecki, L. Nagel-Steger, S. Feuerstein, U. Linne, O. Molt, R. Zadmard, K. Aschermann, M. Wehner, T. Schrader, D. Riesner, Prevention of alzheimer's disease-associated Aβ aggregation by rationally designed nonpeptidic β-Sheet ligands, J. Biol. Chem. 279 (2004) 47497–47505, https://doi.org/10.1074/jbc.M405914200.

[11] G. Bottegoni, M. Veronesi, P. Bisignano, P. Kacker, A.D. Favia, A. Cavalli, Development and application of a virtual screening protocol for the identification of multitarget fragments, ChemMedChem 11 (2016) 1259–1263, https://doi.org/10.1002/cmdc.201500521.

[12] R. Mukherjee, Coordination chemistry with pyrazole-based chelating ligands: molecular structural aspects, Coord. Chem. Rev. 203 (2000) 151–218, https://doi.org/10.1016/S0010-8545(99)00144-7.

[13] T. Takahashi, H. Mihara, Peptide and protein mimetics inhibiting amyloid β-Peptide aggregation, Acc. Chem. Res. 41 (2008) 1309–1318, https://doi.org/10.1021/ar8000475.

[14] R. Singh, A. Panghal, K. Jadhav, A. Thakur, R.K. Verma, C. Singh, M. Goyal, J. Kumar, A.G. Namdeo, Recent advances in targeting transition metals (copper, iron, and zinc) in alzheimer's disease, Mol. Neurobiol. 61 (2024) 10916–10940, https://doi.org/10.1007/s12035-024-04256-8.

[15] S. Colonna, V. Pironti, G. Carrea, P. Pasta, F. Zambianchi, Oxidation of secondary amines by molecular oxygen and cyclohexanone monooxygenase, Tetrahedron 60 (2004) 569–575, https://doi.org/10.1016/j.tet.2003.10.100.

[16] M. Nakajima, Y. Oda, T. Wada, R. Minamikawa, K. Shirokane, T. Sato, N. Chida, Chemoselective reductive nucleophilic addition to tertiary amides, secondary amides, and *N* -methoxyamides, Chem. Eur J. 20 (2014) 17565–17571, https://doi.org/10.1002/chem.201404648.

[17] A.K.L. Fung, W.R. Baker, S. Fakhoury, H.H. Stein, J. Cohen, B.G. Donner, D. S. Garvey, K.P. Spina, S.H. Rosenberg, (1α,2β,3β,4α)-1,2-Bis[[*N* -propyl- *N* -(4-phen- oxybenzyl)amino]carbonyl]cyclobutane- 3,4-dicarboxylic acid (A-87049): a novel potent squalene synthase inhibitor, J. Med. Chem. 40 (1997) 2123–2125, https://doi.org/10.1021/jm970058x.

[18] R. Ma, Y. Gu, Y.-E. Wang, R. Fei, D. Xiong, J. Mao, One-pot synthesis of Indolin-3-ones mediated by $LiN(SiMe_3)_2$/CsF, Org. Lett. 26 (2024) 5082–5086, https://doi.org/10.1021/acs.orglett.4c01265.

[19] H.J. Kumpaty, J.S. Williamson, S. Bhattacharyya, Synthesis of *N* -Methyl secondary amines, Synth. Commun. 33 (2003) 1411–1416, https://doi.org/10.1081/SCC-120018703.

[20] C.J. Lemmerhirt, M. Rombach, A. Bodtke, P.J. Bednarski, A. Link, Oxidation potentials of n-modified derivatives of the analgesic flupirtine linked to potassium K_V7 channel opening activity but not hepatocyte toxicity, ChemMedChem 10 (2015) 368–379, https://doi.org/10.1002/cmdc.201402442.

[21] J.-X. Zhang, L.-Y. Zhang, N.-X. Wang, Y.-H. Wu, Z. Yan, D. Lucan, NMR studies of rotamers with multi-substituted amides, Journal of Engineering Sciences and Innovation 6 (2021) 373–380, https://doi.org/10.56958/jesi.2021.6.4.2.

[22] G.G. Fraga, D.D. Colasurdo, C.C. Santiago, A. Ponzinibbio, L.D. Sasiambarrena, Rotamerization equilibrium in novel N,N-disubstituted chloroacetamides: an NMR spectroscopic study, J. Mol. Struct. 1261 (2022) 132892, https://doi.org/10.1016/j.molstruc.2022.132892.

[23] A. Bisi, R.L. Arribas, M. Micucci, R. Budriesi, A. Feoli, S. Castellano, F. Belluti, S. Gobbi, C. de los Rios, A. Rampa, Polycyclic maleimide-based derivatives as first dual modulators of neuronal calcium channels and GSK-3β for Alzheimer's disease treatment, Eur. J. Med. Chem. 163 (2019) 394–402, https://doi.org/10.1016/j.ejmech.2018.12.003.

[24] D. Perrin, C. Frémaux, A. Shutes, Capillary microfluidic electrophoretic mobility shift assays: application to enzymatic assays in drug discovery, Expet Opin. Drug Discov. 5 (2010) 51–63, https://doi.org/10.1517/17460440903493431.

[25] M.E. Schnute, M.D. McReynolds, T. Kasten, M. Yates, G. Jerome, J.W. Rains, T. Hall, J. Chrencik, M. Kraus, C.N. Cronin, M. Saabye, M.K. Highkin, R. Broadus, S. Ogawa, K. Cukyne, L.E. Zawadzke, V. Peterkin, K. Iyanar, J.A. Scholten, J. Wendling, H. Fujiwara, O. Nemirovskiy, A.J. Wittwer, M.M. Nagiec, Modulation of cellular S1P levels with a novel, potent and specific inhibitor of sphingosine kinase-1, Biochem. J. 444 (2012) 79–88, https://doi.org/10.1042/BJ20111929.

[26] C. Fanslau, D. Pedicord, S. Nagulapalli, H. Gray, S. Pang, L. Jayaraman, J. Lippy, Y. Blat, An electrophoretic mobility shift assay for the identification and kinetic analysis of acetyl transferase inhibitors, Anal. Biochem. 402 (2010) 65–68, https://doi.org/10.1016/j.ab.2010.03.025.

[27] T.J. Wigle, L.M. Provencher, J.L. Norris, J. Jin, P.J. Brown, S.V. Frye, W.P. Janzen, Accessing protein methyltransferase and demethylase enzymology using microfluidic capillary electrophoresis, Chem. Biol. 17 (2010) 695–704, https://doi.org/10.1016/j.chembiol.2010.04.014.

[28] A.W. Sorum, J.H. Shrimp, A.M. Roberts, D.C. Montgomery, N.K. Tiwari, M. Lal-Nag, A. Simeonov, A. Jadhav, J.L. Meier, Microfluidic mobility shift profiling of lysine acetyltransferases enables screening and mechanistic analysis of cellular acetylation inhibitors, ACS Chem. Biol. 11 (2016) 734–741, https://doi.org/10.1021/acschembio.5b00709.

[29] T. Lanyon-Hogg, N.V. Patel, M. Ritzefeld, K.J. Boxall, R. Burke, J. Blagg, A. I. Magee, E.W. Tate, Microfluidic mobility shift assay for real-time analysis of peptide N-Palmitoylation, SLAS Discovery 22 (2017) 418–424, https://doi.org/10.1177/2472555216689529.

[30] S.J. Pollack, K.S. Beyer, C. Lock, I. Müller, D. Sheppard, M. Lipkin, D. Hardick, P. Blurton, P.M. Leonard, P.A. Hubbard, D. Todd, C.M. Richardson, T. Ahrens, M. Baader, D.O. Hafenbradl, K. Hilyard, R.W. Bürli, A comparative study of fragment screening methods on the p38α kinase: new methods, new insights, J. Comput. Aided Mol. Des. 25 (2011) 677–687, https://doi.org/10.1007/s10822-011-9454-9.

[31] D. Perrin, T. Martin, Y. Cambet, C. Frémaux, A. Scheer, Overcoming the hurdle of fluorescent compounds in kinase screening: a case study, assay drug, Dev Technol 4 (2006) 185–196, https://doi.org/10.1089/adt.2006.4.185.

[32] P. Drueckes, Protein Kinase Selectivity Profiling Using Microfluid Mobility Shift Assays, 2016, pp. 143–157, https://doi.org/10.1007/978-1-4939-3673-1_9.

[33] B.D. Wright, C. Simpson, M. Stashko, D. Kireev, E.A. Hull-Ryde, M.J. Zylka, W. P. Janzen, Development of a high-throughput screening assay to identify inhibitors of the lipid kinase PIP5K1C, SLAS Discovery 20 (2015) 655–662, https://doi.org/10.1177/1087057114564057.

[34] H. Xie, L. Lin, L. Tong, Y. Jiang, M. Zheng, Z. Chen, X. Jiang, X. Zhang, X. Ren, W. Qu, Y. Yang, H. Wan, Y. Chen, J. Zuo, H. Jiang, M. Geng, J. Ding, AST1306, A novel irreversible inhibitor of the epidermal growth factor receptor 1 and 2, exhibits antitumor activity both in vitro and in vivo, PLoS One 6 (2011) e21487, https://doi.org/10.1371/journal.pone.0021487.

[35] C.A. Dodson, R. Bayliss, Activation of Aurora-A kinase by protein partner binding and phosphorylation are independent and synergistic, J. Biol. Chem. 287 (2012) 1150–1157, https://doi.org/10.1074/jbc.M111.312090.

[36] M.P. Coghlan, A.A. Culbert, D.A. Cross, S.L. Corcoran, J.W. Yates, N.J. Pearce, O. L. Rausch, G.J. Murphy, P.S. Carter, L. Roxbee Cox, D. Mills, M.J. Brown, D. Haigh, R.W. Ward, D.G. Smith, K.J. Murray, A.D. Reith, J.C. Holder, Selective small molecule inhibitors of glycogen synthase kinase-3 modulate glycogen metabolism and gene transcription, Chem. Biol. 7 (2000) 793–803, https://doi.org/10.1016/S1074-5521(00)00025-9.

[37] D.A.E. Cross, A.A. Culbert, K.A. Chalmers, L. Facci, S.D. Skaper, A.D. Reith, Selective small-molecule inhibitors of glycogen synthase kinase-3 activity protect primary neurones from death, J. Neurochem. 77 (2001) 94–102, https://doi.org/10.1046/j.1471-4159.2001.00251.x.

[38] F.F. Wagner, J.A. Bishop, J.P. Gale, X. Shi, M. Walk, J. Ketterman, D. Patnaik, D. Barker, D. Walpita, A.J. Campbell, S. Nguyen, M. Lewis, L. Ross, M. Weïwer, W. F. An, A.R. Germain, P.P. Nag, S. Metkar, T. Kaya, S. Dandapani, D.E. Olson, A.-L. Barbe, F. Lazzaro, J.R. Sacher, J.H. Cheah, D. Fei, J. Perez, B. Munoz, M. Palmer, K. Stegmaier, S.L. Schreiber, E. Scolnick, Y.-L. Zhang, S.J. Haggarty, E.B. Holson, J. Q. Pan, Inhibitors of glycogen synthase kinase 3 with exquisite kinome-wide selectivity and their functional effects, ACS Chem. Biol. 11 (2016) 1952–1963, https://doi.org/10.1021/acschembio.6b00306.

[39] A. Gandini, M. Bartolini, D. Tedesco, L. Martinez-Gonzalez, C. Roca, N.E. Campillo, J. Zaldivar-Diez, C. Perez, G. Zuccheri, A. Miti, A. Feoli, S. Castellano, S. Petralla, B. Monti, M. Rossi, F. Moda, G. Legname, A. Martinez, M.L. Bolognesi, Tau-centric multitarget approach for alzheimer's disease: development of first-in-class dual glycogen synthase kinase 3β and tau-aggregation inhibitors, J. Med. Chem. 61 (2018) 7640–7656, https://doi.org/10.1021/acs.jmedchem.8b00610.

[40] H. Kroth, A. Ansaloni, Y. Varisco, A. Jan, N. Sreenivasachary, N. Rezaei-Ghaleh, V. Giriens, S. Lohmann, M.P. López-Deber, O. Adolfsson, M. Pihlgren, P. Paganetti, W. Froestl, L. Nagel-Steger, D. Willbold, T. Schrader, M. Zweckstetter, A. Pfeifer, H. A. Lashuel, A. Muhs, Discovery and structure activity relationship of small molecule inhibitors of toxic β-Amyloid-42 fibril formation, J. Biol. Chem. 287 (2012) 34786–34800, https://doi.org/10.1074/jbc.M112.357665.

[41] S.R. Chowdhury, F. Xie, J. Gu, L. Fu, Small-molecule amyloid beta-aggregation inhibitors in alzheimer's disease drug development, Pharmaceutical Fronts 01 (2019) e22–e32, https://doi.org/10.1055/s-0039-1698405.
[42] M. Bartolini, M. Naldi, J. Fiori, F. Valle, F. Biscarini, D.V. Nicolau, V. Andrisano, Kinetic characterization of amyloid-beta 1–42 aggregation with a multimethodological approach, Anal. Biochem. 414 (2011) 215–225, https://doi.org/10.1016/j.ab.2011.03.020.
[43] M. Bartolini, C. Bertucci, M.L. Bolognesi, A. Cavalli, C. Melchiorre, V. Andrisano, Insight into the kinetic of amyloid β (1–42) peptide self-aggregation: elucidation of inhibitors' mechanism of action, Chembiochem 8 (2007) 2152–2161, https://doi.org/10.1002/cbic.200700427.
[44] N. Das, J. Raymick, S. Sarkar, Role of metals in Alzheimer's disease, Metab. Brain Dis. 36 (2021) 1627–1639, https://doi.org/10.1007/s11011-021-00765-w.
[45] M.L. Hegde, P. Bharathi, A. Suram, C. Venugopal, R. Jagannathan, P. Poddar, P. Srinivas, K. Sambamurti, K.J. Rao, J. Scancar, L. Messori, L. Zecca, P. Zatta, Challenges associated with metal chelation therapy in alzheimer's disease, J. Alzheim. Dis. 17 (2009) 457–468, https://doi.org/10.3233/JAD-2009-1068.
[46] R. Squitti, M.C.A. Rongioletti, G. Liguri, Copper, oxidative stress, Alzheimer's disease, and dementia, in: Vitamins and Minerals in Neurological Disorders, Elsevier, 2023, pp. 65–85, https://doi.org/10.1016/B978-0-323-89835-5.00030-2.
[47] H.W. Ejaz, W. Wang, M. Lang, Copper toxicity links to pathogenesis of alzheimer's disease and therapeutics approaches, Int. J. Mol. Sci. 21 (2020) 7660, https://doi.org/10.3390/ijms21207660.
[48] P.J. Crouch, L.W. Hung, P.A. Adlard, M. Cortes, V. Lal, G. Filiz, K.A. Perez, M. Nurjono, A. Caragounis, T. Du, K. Laughton, I. Volitakis, A.I. Bush, Q.-X. Li, C. L. Masters, R. Cappai, R.A. Cherny, P.S. Donnelly, A.R. White, K.J. Barnham, Increasing Cu bioavailability inhibits Aβ oligomers and tau phosphorylation, Proc. Natl. Acad. Sci. 106 (2009) 381–386, https://doi.org/10.1073/pnas.0809057106.
[49] P. Agarwal, S. Ayton, S. Agrawal, K. Dhana, D.A. Bennett, L.L. Barnes, S. E. Leurgans, A.I. Bush, J.A. Schneider, Brain copper may protect from cognitive decline and Alzheimer's disease pathology: a community-based study, Mol. Psychiatr. 27 (2022) 4307–4313, https://doi.org/10.1038/s41380-022-01802-5.
[50] A. Contestabile, Cerebellar granule cells as a model to study mechanisms of neuronal apoptosis or survival in vivo and in vitro, Cerebellum 1 (2002) 41–55, https://doi.org/10.1080/147342202753203087.
[51] F. Leng, P. Edison, Neuroinflammation and microglial activation in Alzheimer disease: where do we go from here? Nat. Rev. Neurol. 17 (2021) 157–172, https://doi.org/10.1038/s41582-020-00435-y.
[52] E. Peña-Altamira, S. Petralla, F. Massenzio, M. Virgili, M.L. Bolognesi, B. Monti, Nutritional and pharmacological strategies to regulate microglial polarization in cognitive aging and alzheimer's disease, Front. Aging Neurosci. 9 (2017), https://doi.org/10.3389/fnagi.2017.00175.
[53] G. Zhang, J.-L. He, X.-Y. Xie, C. Yu, LPS-induced iNOS expression in N9 microglial cells is suppressed by geniposide via ERK, p38 and nuclear factor-κB signaling pathways, Int. J. Mol. Med. 30 (2012) 561–568, https://doi.org/10.3892/ijmm.2012.1030.
[54] S. Carmona, K. Zahs, E. Wu, K. Dakin, J. Bras, R. Guerreiro, The role of TREM2 in Alzheimer's disease and other neurodegenerative disorders, Lancet Neurol. 17 (2018) 721–730, https://doi.org/10.1016/S1474-4422(18)30232-1.
[55] Y. Zhao, S. Bhattacharjee, B.M. Jones, P. Dua, P.N. Alexandrov, J.M. Hill, W. J. Lukiw, Regulation of TREM2 expression by an NF-κB-sensitive miRNA-34a, Neuroreport 24 (2013) 318–323, https://doi.org/10.1097/WNR.0b013e32835fb6b0.
[56] J. Bicker, G. Alves, A. Fortuna, P. Soares-da-Silva, A. Falcão, A new PAMPA model using an in-house brain lipid extract for screening the blood–brain barrier permeability of drug candidates, Int. J. Pharm. 501 (2016) 102–111, https://doi.org/10.1016/j.ijpharm.2016.01.074.
[57] M. Etxebeste-Mitxeltorena, E. Niza, C.M. Fajardo, C. Gil, L. Gómez-Gómez, A. Martinez, O. Ahrazem, Neuroprotective properties of exosomes and chitosan nanoparticles of Tomafran, a bioengineered tomato enriched in crocins, Nat Prod Bioprospect 14 (2024) 9, https://doi.org/10.1007/s13659-023-00425-9.
[58] L. Di, E.H. Kerns, K. Fan, O.J. McConnell, G.T. Carter, High throughput artificial membrane permeability assay for blood–brain barrier, Eur. J. Med. Chem. 38 (2003) 223–232, https://doi.org/10.1016/S0223-5234(03)00012-6.
[59] A. Martinez, D. Perez, C. Gil, Lessons learnt from glycogen synthase kinase 3 inhibitors development for alzheimer's disease, Curr. Top. Med. Chem. 13 (2013) 1808–1819, https://doi.org/10.2174/15680266113139990138.
[60] H. Naiki, K. Higuchi, K. Nakakuki, T. Takeda, Kinetic analysis of amyloid fibril polymerization in vitro, Lab. Invest. (1991) 104–110.